the plant journal

SEB SOCIETY FOR EXPERIMENTAL BIOLOGY

The Plant Journal (2025) **123,** e70289 doi: 10.1111/tpj.70289

Arabidopsis Vacuolar protein sorting 9a (VPS9a) is required for glutamine synthetase/glutamate synthase (GS/GOGAT) cycle and autophagy under nutrient starvation

Baiyang Yu[1,2,3], Yanhui Zhou[2,4], Yunfeng Shi[2], Shengshu Wang[2,5], Qing Pang[2,4], Chao Yang[2,4], Thomas Roitsch[3], Weiming Hu[2,*], Yizhou Wang[1,*] and Fen Liu[2,*]

[1]*Institute of Crop Science, College of Agriculture and Biotechnology, Zhejiang University, Hangzhou 310058, China,*
[2]*Lushan Botanical Garden, Jiangxi Province and Chinese Academy of Sciences, Jiujiang 332900, China,*
[3]*Department of Plant and Environmental Sciences Section for Crop Sciences, University of Copenhagen, Taastrup DK-2630, Denmark,*
[4]*School of Life Sciences, Nanchang University, Nanchang 330031, China, and*
[5]*College of Forestry, Northwest A&F University, Yangling 712100, China*

Received 19 December 2024; revised 6 May 2025; accepted 9 June 2025.
*For correspondence (e-mail huwm@lsbg.cn and wangyizhou@zju.edu.cn and liuf@lsbg.cn).

SUMMARY

Plants have developed complex endomembrane systems in response to environmental challenges such as nutrient deficiency. This study focused on the role of *Vacuolar protein sorting 9 (VPS9a)*, a key regulatory gene involved in the endosomal sorting process in *Arabidopsis thaliana*. Loss of *VPS9a* function results in stress-sensitive phenotypes under carbon and nitrogen starvation. First, we investigated the changes in the Glutamine Synthetase/Glutamate Synthase (GS/GOGAT) cycle under nitrogen starvation and conducted a co-expression network analysis based on transcriptomic profiles. These results indicate that the endocytic pathway and the majority of the degradation processes are related to GS and NADH-GOGAT activity. Genes related to autophagy and endocytic pathways showed diverse response trends in Col-0, *vps9a-2*, and *35S: VPS9a-GFP/vps9a-2*. Several autophagy- and endocytosis-related genes, including *Autophagy-related protein 1* (*ATG1*), *Autophagy-related protein 8* (*ATG8*), *Thylakoid lumen protein* (*TLP18.3*), *Autoinhibited Ca(2+)-ATPase, Isoform 4* (*ACA4*), *MAP kinase 2* (*AtMKK2*), and *Extensin 21* (*EXT21*), were identified as hub genes. Further, we found that the loss of *VPS9a* function leads to reduced accumulation of autophagic bodies and a marked decrease in ATG8a protein levels but does not affect autophagic flux or the accumulation of ATG8 with phosphatidylethanolamine (PE). Interestingly, *VPS9a* appears to exert differential effects on various ATG8 Homologs. In summary, our results established a connection between autophagy, endocytic pathways, and nitrogen metabolism processes, identifying key hub genes involved in these processes. Among these hub genes, *VPS9a* was found to affect ATG8a levels, suggesting that *VPS9a* selectively regulates specific ATG8 proteins involved in autophagic processes.

Keywords: vacuolar protein sorting 9 (VPS9a), glutamine synthetase/glutamate synthase (GS/GOGAT) cycle, nutrient deprivation, autophagy, endocytosis.

INTRODUCTION

Endocytosis and endosomal trafficking are the basic recycling requirements for cellular cargo trafficking (Paez Valencia et al., 2016). In plants, the primary protein sorting pathway proceeds from the endoplasmic reticulum (ER)/plasma membrane (PM) to the vacuole/lysosomes (Reyes et al., 2011), the endosomal sorting complexes required for transport (ESCRT) are then responsible for substrate sorting and driving the cargo into intraluminal vesicles (ILVs) (Gao et al., 2014). In addition, the prevacuolar compartments, multivesicular bodies (MVBs), and late endosome degradation depend on ESCRTs for vacuolar fusion (Henne et al., 2011). *Vacuolar protein sorting 9* (*VPS9*) is a key GTPase guanine-nucleotide exchange factor (GEF) involved in the endosomal transport process (Wen et al., 2015). In Arabidopsis, two homologous genes encode VPS9. Among them, *VPS9b* is expressed in pollen and embryos but is difficult to detect in Arabidopsis seedlings (Goh et al., 2007; Hao et al., 2024; Rajagopal & Mathew, 2020). Additionally, the *VPS9b* mutant does not

exhibit any observable phenotypic defects. In contrast, *VPS9a* plays a predominant role in vegetative growth and is crucial for regulating endosomal trafficking (Ito et al., 2018; Sunada et al., 2016). It encodes an RAB5-specific GEF and is constitutively expressed in most tissues (Goh et al., 2007). Arabidopsis contains three homologous genes for RAB5 GTPases: *RHA1*, *ARA7*, and *ARA6* (Ito et al., 2018). RHA1 and ARA7 are conventional Rab5 proteins with conserved functions, whereas ARA6, a plant-specific RAB5, competitively inhibits the endosomal transport processes of canonical RAB5 members (Ebine et al., 2011; Ito et al., 2018). Expression of $ARA7^{Q69L}$ (ATP-fix type) or inactivation of *ARA6* represses the defective phenotype of a *vps9a-2* mutant (Ebine et al., 2011, Ito et al., 2018). In yeast and mammals, VPS9-domain proteins with RAB5 GTPases are involved in autophagosome (AP) maturation. Loss of *VPS9* function inhibits autophagic flux (Li et al., 2019; Zhou et al., 2017) and leads to the accumulation of abnormal autophagosome (AP) structures (Hargrove-Grimes et al., 2020), which may affect plant nutrient metabolism and recycling processes.

Nitrogen is a fundamental element required for plant growth and development (Masclaux-Daubresse et al., 2010; The et al., 2020). Nitrogen assimilation in plants transforms inorganic nitrogen (primarily nitrate and ammonium) into organic nitrogen compounds (Xing et al., 2023). Inorganic nitrogen absorbed by plants is initially reduced to nitrite through the action of nitrate reductase, and is subsequently converted to ammonium (NH_4^+) by nitrite reductase (Krapp, 2015). The resulting NH_4^+ is then assimilated through the glutamine synthetase (GS) and glutamate synthase (GOGAT) cycle, which converts inorganic nitrogen into organic forms (Balotf et al., 2016; Zhang et al., 2025). In this pathway, GS catalyzes the incorporation of Ammonium into glutamate (Glu) to form glutamine (Gln), whereas GOGAT facilitates the transfer of an amide group from Gln to 2-oxoglutarate (2-OG), resulting in the production of two molecules of Glu (Li, Nian, et al., 2022; Zhang et al., 2019). The Glu and Gln produced in the GS/GOGAT cycle serve as precursors for the biosynthesis of other amino acids such as aspartate (Asp), proline (Pro), and arginine (Arg) (Liu et al., 2022). These amino acids can be used to synthesize proteins and other nitrogen-containing organic compounds (Oliveira et al., 2001). Moreover, nitrogen assimilation is tightly regulated by genetic and environmental factors to ensure efficient nitrogen utilization and balanced plant growth (Masclaux-Daubresse et al., 2010; Zhang et al., 2025), and a lack of nitrogen in the environment affects its assimilation in plants (Hodges, 2002; Xing et al., 2023). Physiological and metabolic evidence indicates that amino acid metabolism within the GS/GOGAT cycle is highly responsive to nitrogen availability (Lemaitre et al., 2008). Under nitrogen-limited conditions, accelerated protein degradation increases NH_4^+ production, which in turn enhances GS activity (del Mar Rubio-Wilhelmi et al., 2012). Prolonged nitrogen starvation results in a progressive decline in endogenous amino acid levels (Cruz et al., 2004; Kovácik et al., 2006), suggesting a disruption of nitrogen assimilation and utilization. Furthermore, nitrogen deprivation activates the autophagy pathway, facilitates protein degradation and nitrogen recycling to maintain cellular nitrogen homeostasis, and supports plant adaptations to nitrogen stress (Cao et al., 2022; Li et al., 2015; Marshall & Vierstra, 2018). These findings suggest a potential functional link between autophagy and the GS/GOGAT cycle in plants.

As one of the major cytoplasmic material turnover pathways, autophagy is a conserved process involved in the development of coping mechanisms for environmental challenges (Liao & Bassham, 2020; Tang & Bassham, 2022). During autophagic vesicle delivery, the targeted components are engulfed into a double-membrane structure and interact with early or late endosomes to form amphisomes (Javed et al., 2023; Zhao et al., 2022), which are then transported to the vacuole lumen/lysosome where the cargo is released for degradation (Li & Vierstra, 2012; Zhou et al., 2022). Genetic and cellular evidence indicates that autophagy plays a vital role in nitrogen assimilation in Arabidopsis and other crops (Erlichman et al., 2023; Li et al., 2015; Masclaux-Daubresse et al., 2010), particularly in the adaptation to low-nitrogen environments (Chung et al., 2009; Fan et al., 2020; Suttangkakul et al., 2011). Autophagy enhances nitrogen uptake and the photosynthetic rate under low-nitrogen conditions, thereby improving productivity (Cao et al., 2022; Sun et al., 2018). Moreover, autophagy is important for nitrogen remobilization (Di Berardino et al., 2018; Erlichman et al., 2023; Fan et al., 2020), For example, ribulose-1,5-bisphosphate carboxylase/oxygenase (Rubisco) in leaves contains a significant amount of nitrogen, and the degradation process depends on autophagic transport (Izumi et al., 2010). Autophagy defects affect reproductive growth, which is characterized by biomass reduction, premature leaf senescence, and decreased yield (Fan et al., 2020; Kurusu et al., 2014; Thompson et al., 2005; Wada et al., 2015).

Emerging evidence supports the crosstalk between endosomal trafficking and autophagy regulation in Arabidopsis (Gao et al., 2017; Isono, 2021). Several key endocytic components are involved in the regulation of autophagy. Studies have revealed that the functional loss of components of the phosphoinositide 3-kinase (PI3K) complex leads to typical endosomal sorting defect phenotypes such as those with developmental defects, sterility, abnormal accumulation of vacuolar storage proteins, and irregular distribution of auxin-signaling PIN-FORMED proteins in the roots (Lee et al., 2008; Leprince et al., 2014; Liu et al., 2018; Xu et al., 2011). Additionally, PI3K complex

components regulate autophagic flux and the accumulation of autophagic bodies in the vacuole lumen (Liu et al., 2018; Liu et al., 2020; Wang et al., 2022; Xu et al., 2011). Moreover, AP delivery relies on the FYVE domain protein required for endosomal sorting 1 (FREE1), SH3 domain containing protein 2 (SH3P2), and the CELL DEATH-RELATED ENDOSOMAL FYVE/SYLF PROTEIN1 (CFS1), all of which function in endosomal sorting (Gao et al., 2015; Sutipatanasomboon et al., 2017; Zhuang et al., 2013). A recent study indicated that CFS1 functions as a receptor for ATG8 and together with the ESCRT-I component VPS23A, regulates autophagic flux in plants (Zhao et al., 2022), establishing a connection between core ESCRT components and selective autophagy pathways. Additionally, endocytosis-regulating proteins are involved in the transport of AP, and soluble *N*-ethylmaleimide-sensitive factor attachment receptor proteins (SNAREs) are essential for AP fusion with the tonoplast. Abnormal AP structures accumulate outside the tonoplast in mutants of specific SNAREs, such as *VAMP724*/*VAMP726*, and *VTI12*, indicating a failure in the fusion process (He et al., 2023; Surpin et al., 2003). These studies indicated the strong correlation between vacuolar trafficking and the autophagic degradation process.

Extensive evidence supports the various functions of endosome transportation, including innate immunity, abiotic stress, and development (Baral et al., 2015; Nielsen et al., 2017; Rajagopal & Mathew, 2020). Our understanding of the molecular mechanisms involved in plant responses to nutrient stress and the role of endosomal sorting pathway components in the regulation of nitrogen metabolism and autophagy remains limited. In this study, we revealed that the key gene *VPS9a* in ESCRTs affects the activity of key enzymes involved in nitrogen metabolism. Loss of *VPS9a* function leads to a hypersensitive response to nutrient stress. At the transcriptional level, we identified key pathways involved in the GS/GOGAT cycle and hub genes involved in autophagy and endocytosis. Further validation of *VPS9a* function in autophagy revealed its potential role in the protein level of ATG8s and autophagic body accumulation under starvation. These results indicated that *VPS9a* is important for the regulation of autophagy.

RESULTS

VPS9a functional loss leads to hypersensitive response to carbon and nitrogen limitation

The homologous protein of plant VPS9a in yeast and *Pyricularia oryzae* is crucial for the regulation under nutrient limitation and participates in autophagy (Zhu *et al.*, 2018, Li et al., 2019). To determine whether VPS9a controls these processes in plants, we examined the phenotype of *vps9a-2* mutants under various nutritional conditions. The survival rate of *vps9a-2* decreased by approximately 30% compared to Columbia-0 (Col-0) on the 5th day under carbon starvation (Figure 1a,b), whereas *35S:VPS9a-GFP/-vps9a-2* lines and *VPS9apro:VPS9a-GFP/vps9a-2* exhibited similar phenotypes and survival rates to Col-0 (Figure 1a, Figure S1). Moreover, *vps9a-2* exhibited enhanced sensitivity on the 7th day (Figure 1a). In nitrogen-deficient medium, *vps9a-2* displayed early senescence (Figure 1c) and reduced chlorophyll content (Figure 1d), whereas the two overexpression lines had similar phenotypes and endogenous chlorophyll levels compared with that of the Col-0 (Figure 1d). These findings indicate that VPS9a-dependent processes affect Arabidopsis response to nutrient deprivation.

We further investigated the enzymatic activities of GS and NADH-GOGAT, which are involved in nitrogen metabolism. The results showed that GS activity was upregulated under nitrogen starvation. Specifically, after 48 h, GS activity in *vps9a-2* increased 2.17-fold and 1.83-fold compared to that of Col-0 and *35S:VPS9a-GFP/vps9a-2*, respectively (Figure 1e). After 96 h, the GS activity in Col-0 and *35S:VPS9a-GFP/vps9a-2* showed no significant changes compared to that expressed at 48 h, whereas *vps9a-2* remained at a significantly higher GS level than that of the other two lines. Additionally, *vps9a-2* exhibited higher NADH-GOGAT activity under normal conditions and sustained elevated levels after 96 h of treatment, with a 2.87-fold increase compared with that of Col-0 (Figure 1f).

Because the GS/GOGAT cycle is essential for amino acid metabolism (Figure S2a), we further analyzed the endogenous levels of relevant amino acids, including Gln, Glu, Asp, Arg, and Pro. Most amino acids were downregulated in *vps9a-2* (Figure 1g–i, Figure S2b). The Gln was significantly higher in *vps9a-2* at 48 h and 96 h under nitrogen deprivation (-N) conditions than in Col-0 and *35S:VPS9a-GFP/vps9a-2* (Figure 1g). Moreover, the mutant accumulated more Glu under normal conditions (0 h) compared with the treatments, showing a significant difference from Col-0 at 96 h (Figure 1h). The Asp levels showed a similar trend, but no significant changes were observed in Col-0 during the -N treatment period (Figure 1i). Asp levels also showed overaccumulation in *vps9a-2* at 0 h, with a rapid response to the -N treatment, resulting in considerable decreases at 48 and 96 h (Figure 1i).

The biosynthesis of Arg and Pro relies on the GS/GOGAT cycle, in which glutamine serves as a major nitrogen donor in amino acid biosynthesis (Figure S2a–c). Arg levels decreased in all three lines (Figure S2b), whereas Pro levels were upregulated only in *vps9a-2* (Figure S2c). These findings suggest that the *vps9a* mutation affects nitrogen recycling in Arabidopsis by modulating the GS/GOGAT cycle activity. The distinct enzyme activity responses and differential amino acid accumulation patterns detected in the three lines highlight the diversity of nitrogen remobilization processes during starvation.

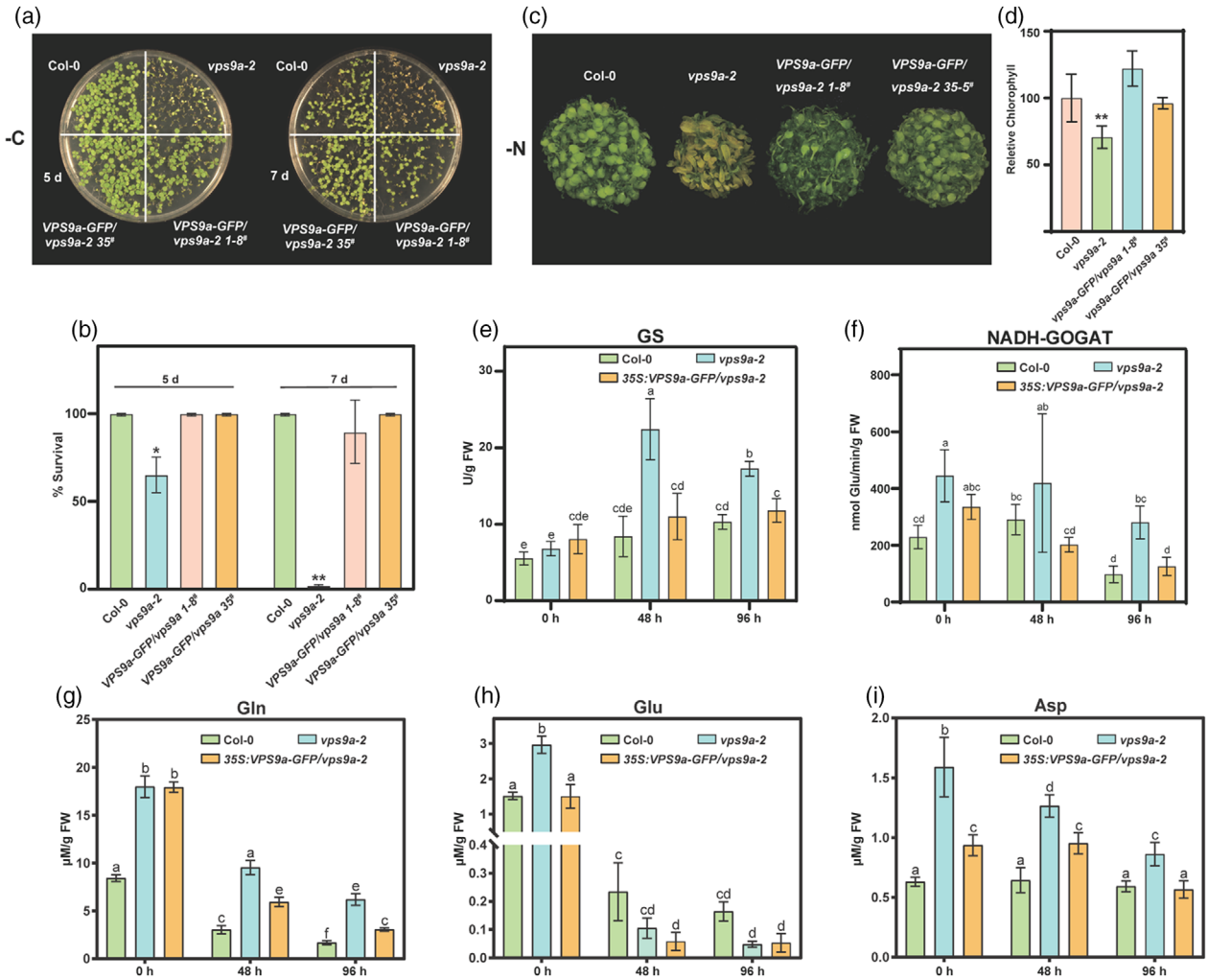

Figure 1. *VPS9a* function in tolerance to nutritional stress and key enzyme activities related to nitrogen assimilation.
(a) Carbon starvation treatment. Plants were grown on glucose-free MS solid medium for 10 days (16 h light/8 h dark), then transferred to a dark environment for an additional 5 or 7 days.
(b) Survival rates of seedlings after recovery from carbon starvation. Data represent mean ± SDs (n = 3). Asterisks indicate significant differences compared to WT (n = 3; *P < 0.05; **P < 0.01; Student's t-test).
(c) Nitrogen starvation treatment. Col-0, *vps9a-2*, and complemented lines were initially cultivated in MS liquid medium for 1 week. Subsequently, the medium was replaced with nitrogen-free (-N) liquid medium for an additional week.
(d) Relative chlorophyll content under nitrogen starvation. Data were normalized to the Col-0 and respected by mean ± SD (n = 3; *P < 0.05; **P < 0.01; Student's t-test).
(e, f) Glutamine synthetase (GS) (e) and NADH-dependent glutamate synthase (NADH-GOGAT) (f) activity of Col-0, *vps9a-2*, and *35S:VPS9a-GFP/vps9a-2* seedlings after 0, 48, and 96-h nitrogen starvation. Enzyme activity is expressed relative to fresh weight (n = 4, P < 0.05, Student's t-test).
(g) Glutamine (Gln) content. (h) Glutamate (Glu) content. (i) Aspartate (Asp) content. Amino acid contents are expressed relative to fresh weight (n = 6, P < 0.05, Student's t-test).

Construction of a co-expression network and identification of key modules associated with GS/GOGAT activity

To understand the function of *VPS9a* in transcriptional changes under -N conditions and identify key regulatory pathways, we performed transcriptional profiling of Col-0, *vps9a-2*, and *35S:VPS9a-GFP/vps9a-2 35–5#* under -N treatment at 0, 48, and 96 h. Principal Component Analysis (PCA) showed that the 0 h treatment samples clearly separated from those of the 48 and 96 h treatment on PC1, which explained 86.4% of the variance (Figure S3a), thus indicating a significant impact of -N treatment on transcriptional levels.

To identify the key modules involved in the GS/GOGAT cycle under low-nitrogen stress conditions, a weighted gene co-expression network analysis (WGCNA) was constructed based on the gene expression data of all genes at different stages in Col-0, *vps9a-2*, and *35S:VPS9a-GFP/vps9a-2*. After removing low-quality and

low-expression data, 23 928 genes in Col-0 (Table S2), 23 897 in *vps9a-2* (Table S3) and 23 811 in *35S:VPS9a-GFP/vps9a-2* (Table S4) were used to construct the co-expression network. Using $\beta = 8$ as the soft-threshold power (Figure S4a–c), genes were grouped into 20 different modules in *vps9a-2*, while 19 modules were identified in Col-0 and *35S:VPS9a-GFP/vps9a-2* using the dynamic tree cutting method (Figure S3b–d). The numbers of genes corresponding to these modules are shown in Figure S5.

Subsequently, we identified the key modules related to GS and NADH-GOGAT activity via eigengene–trait correlation analysis (Gan *et al.*, 2023). In Col-0, the brown module was significantly associated with the activities of both enzymes. The turquoise and blue modules were specifically linked to GS enzyme activity, whereas four modules (pink, brown, dark red, and red) showed significant correlations with NADH-GOGAT enzyme activity (Figure S6a). The Kyoto Encyclopedia of Genes and Genomes (KEGG) enrichment analysis revealed that genes within the blue module were primarily involved in transport processes such as endocytosis, protein processing in the endoplasmic reticulum, and protein export (Figure S7a). Furthermore, the brown and turquoise modules were enriched in pathways related to essential degradation processes (e.g., autophagy and proteasome degradation), photosynthesis, and carbon metabolism (Figure S7b,c). The pink module was particularly enriched in the plant hormone signal transduction pathways (Figure S7d), whereas the dark red and red modules showed no significant pathway enrichment. Notably, the same pathways were identified in the blue, turquoise, and purple modules of *35S:VPS9a-GFP/vps9a-2* (Figures S6b and S8a–c).

In *vps9a-2*, six modules exhibited significant correlations (Figure S6c), comprising three positively correlated (orange, black, and brown) and three negatively correlated (cyan, light cyan, and light green) modules. The orange module lacked significantly enriched pathways. In contrast, the other positively correlated modules included pathways similar to those in Col-0 and *35S:VPS9a-GFP/vps9a-2*, including autophagy and protein export, along with specific pathways, such as DNA replication, base excision repair, and vitamin B6 metabolism, which were uniquely enriched in the black module (Figure S9a,b). In the negatively correlated modules, genes were notably associated with isoquinoline alkaloid metabolism, plant circadian rhythm and ubiquitin-mediated proteolysis (Figure S9c–e). Of the three modules associated with NADH-GOGAT activity (Figure S6c), the dark turquoise module was involved in ubiquitin-mediated proteolysis and protein processing in the endoplasmic reticulum (Figure S9f), whereas the magenta and blue modules were significantly associated with genes involved in the proteasome, endocytosis, and autophagy (Figure S9g,h). These results highlight the critical roles of transport and degradation processes in plant responses to low-nitrogen conditions, underscoring their central functions in the regulation of GS and NADH-GOGAT activities.

VPS9a impacts autophagy and endocytic gene responses during nitrogen deprivation

Given that the endocytosis-mediated transport and autophagy-enriched modules were significantly correlated with GS and NADH-GOGAT activity, these pathways were identified as regulators of low-nitrogen metabolism. To validate this, we investigated the expression trends of autophagy- and endocytosis-related genes across the three lines (Table S5 and Table S6, respectively). Overall, the autophagy-related genes were upregulated under N stress. In Col-0, two profile modules were significantly enriched (Figure 2a), with profile 7 showing the highest enrichment. Genes in this module were consistently upregulated at 48 and 96 h, whereas profile 4 contained 14 autophagy genes that were significantly upregulated at 96 h (Figure 2a). In *vps9a-2*, profile 4 exhibited the most pronounced enrichment, followed by profile 7 (Figure 2b), which collectively harbored 21 autophagy genes (13 in profile 4 and 8 in profile 7). Conversely, in the *35S:VPS9a-GFP/vps9a-2* line, only profile 7 was significantly enriched, comprising 23 of the 32 autophagy genes identified (Figure 2c).

Endocytic genes exhibited upregulation patterns in both Col-0 (Figure 2d) and *35S:VPS9a-GFP/vps9a-2* line (Figure 2f), with the majority showing increased expression at 48 and 96 h across profiles 4, 6, and 7. In *vps9a-2*, these genes were significantly enriched in profiles 6 and 7 (Figure 2e), accounting for 88 of the 117 (75.2%) identified endocytic genes.

In summary, these results demonstrate that *VPS9a* significantly affects the gene expression response in autophagy and endocytosis during nitrogen starvation. Overexpression of *VPS9a* resulted in a significant induction of autophagy-related genes under stress conditions. Furthermore, while most endocytic genes responded to nitrogen deficiency, the *vps9a-2* mutant exhibited accelerated transcriptional responses, as evidenced by significant upregulation within the initial 48-h period.

Identified hub genes related to autophagy and endocytic pathways

Hub genes were determined based on the gene interaction networks (Figure 3). Four hub genes were found in the autophagy pathway. *ATG8a* (AT4G21980) emerged as a central regulatory gene in both Col-0 and *35S:VPS9a-GFP/vps9a-2* networks (Figure 3a,c). *ATG8b* (AT4G04620) functioned as a hub gene in both *vps9a-2* and *35S:VPS9a-GFP/vps9a-2* (Figure 3b,c). Additionally, *ATG1a* (AT3G61960) and *ATG1b* (AT3G53930) were uniquely identified as hub genes in the *vps9a-2* network (Figure 3b). The ATG8 family encodes ubiquitin-like proteins that are

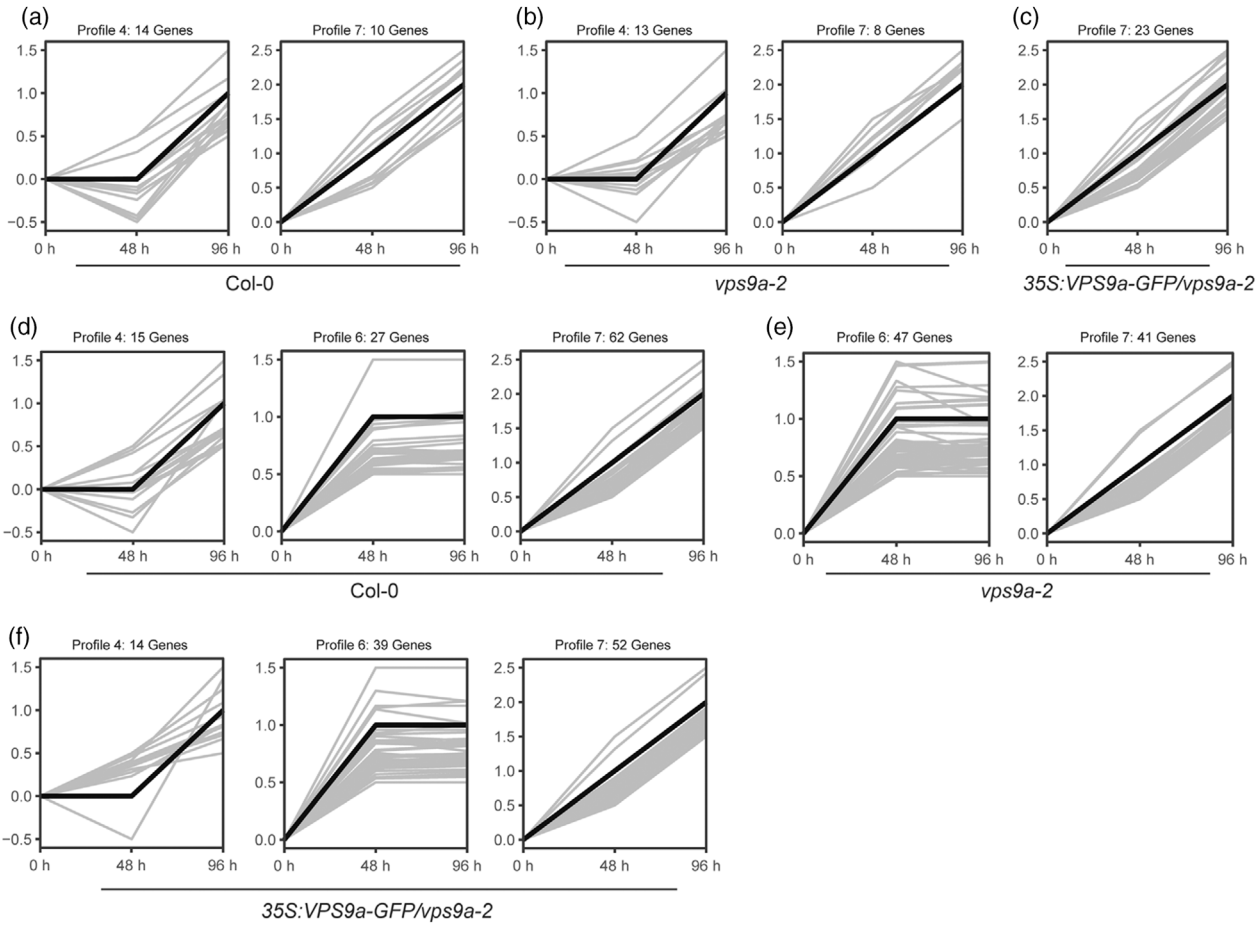

Figure 2. Profile model analysis of autophagy and endocytic genes during -N stress.
(a–c) Profile model analysis of autophagy-related gene expression of Col-0 (a), *vps9a-2* (b), and *35S:VPS9a-GFP/vps9a-2* (c). Significant enriched profile models are displayed ($P < 0.05$).
(d–f) Profile model analysis of endocytic gene expression of Col-0 (d), *vps9a-2* (e), and *35S:VPS9a-GFP/vps9a-2* (f). Significant enriched profile models are displayed ($P < 0.05$).

important for cargo selection, transport, and degradation (Javed et al., 2023; Johansen & Lamark, 2020; Kellner et al., 2017). Similarly, *ATG1* encodes a Ser/Thr kinase that functions as a component of the autophagy initiation complex and positively regulates phagophore formation (Li & Vierstra, 2014; Suttangkakul et al., 2011). These findings highlight the essential roles of ATG1 and ATG8 homologs in autophagy under nitrogen stress and reveal their involvement in maintaining cellular homeostasis during nutrient deprivation.

In the endocytic gene interaction network of wild-type Col-0, we identified key hub genes comprising *ALIX* (AT1G15130), *ACA4* (AT2G41560), *TLP18.3* (AT1G54780), *ATMKK2* (AT4G29810), *VPS4* (AT2G27600), *VPS37* (AT3G53120), *EXT21* (AT2G43150), and *VPS2.1* (AT2G06530) (Figure 3d). Notably, the *vps9a-2* mutant network featured the gene encoding ADL3 (AT1G59610), a GTPase implicated in clathrin-coated endocytosis (Ekanayake *et al.*, 2021, Gnyliukh *et al.*, 2024) as the most connected hub gene (Figure 3e). Similarly, *35S:VPS9a-GFP/vps9a-2* displayed four hub genes, *ALIX* (AT1G15130), *SNF7.1* (AT4G29160), *VPS4* (AT2G27600), and *VPS29* (AT3G47810) (Figure 3f).

These hub genes included core components of the ESCRT machinery. Among them, *VPS37* is a part of ESCRT-I (Boura et al., 2011; Spallek et al., 2013), *VPS2* and *SNF7* belong to ESCRT-III (Hilscher et al., 2016; Ibl et al., 2012) and ALIX and VPS4 function as ESCRT-III-associated proteins (Cardona-Lopez et al., 2015; Reyes et al., 2014). In addition, *VPS29*, a component of the retromer complex (Jha & Larson, 2023), mediates the retrograde transport of transmembrane cargo from endosomes to the Golgi complex (Buser & Spang, 2023; Jha & Larson, 2023). The remaining hub genes encode proteins that exhibit diverse functions–ACA4, localized to vacuolar membranes, is implicated in calcium homeostasis, gas exchange, and biotic stress responses (Boursiac et al., 2010; Hilleary et al., 2020); *TLP18.3* encodes a

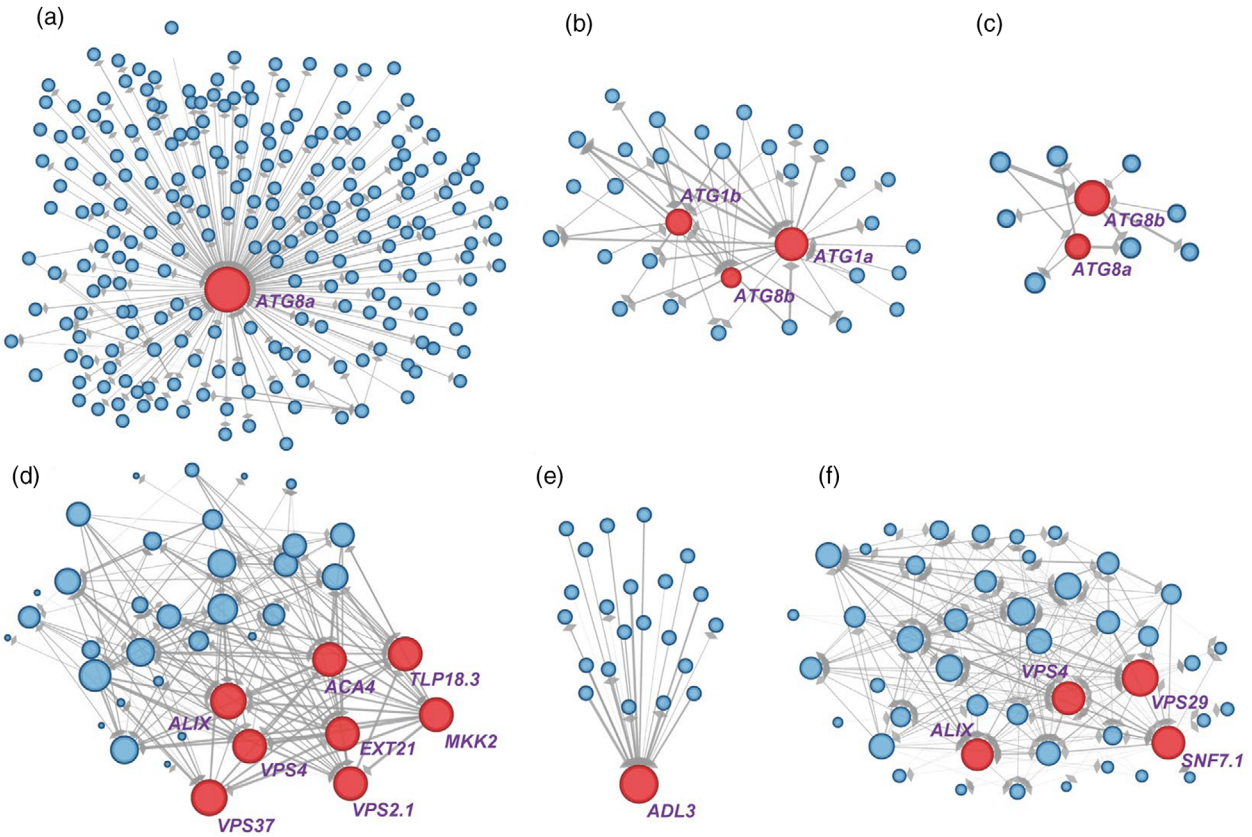

Figure 3. Identified hub genes involved in autophagy and endocytic pathways.
(a–c) Interaction network of autophagy-related genes of Col-0 (a), *vps9a-2* (b), and *35S:VPS9a-GFP/vps9a-2* (c).
(d–f) Interaction network of endocytic genes of Col-0 (d), *vps9a-2* (e), and *35S:VPS9a-GFP/vps9a-2* (f). Each node represents an interacting gene, with the red-colored nodes indicating hub genes. The size of the node indicates the degree value of the gene in the interaction network. The thickness of lines between genes represents the strength of their correlation (weight value).

thylakoid lumen protein involved in photosystem II processes (Jarvi et al., 2016); *ATMKK2*, a MAP kinase, functions in plant immunity, growth, development, and abiotic stress response (Siodmak et al., 2023; Takagi et al., 2019) whereas the function of *EXT21* remains uncharacterized. Collectively, these hub genes are critical regulators of endocytosis and play potential roles in nitrogen stress.

VPS9a modulates ATG8a protein level and autophagic body accumulation under nutrient deficiency

As mentioned above, *vps9a-2* influences the response of autophagy-related genes. In the gene interaction network, *ATG8* and its homologs appeared as core genes involved in the autophagic response to nitrogen stress. To further explore the molecular mechanism which *VPS9a* regulates autophagy, we analyzed the expression levels of *ATG8* homologs in *vps9a-2* and Col-0 in both Murashige and Skoog (MS) medium (Figure 4a) and under nutrient-limited conditions (Figure 4b,c). qRT-PCR analysis revealed that *ATG8a*, *ATG8e*, *ATG8f*, and *ATG8h* were significantly upregulated in *vps9a-2* compared with Col-0 during nutrient starvation, whereas *ATG8g* displayed markedly low-expression levels (Figure 4b,c). Additionally, *ATG2*, *ATG6*, and *ATG7* showed increased expression in *vps9a-2*, with patterns distinct from those in Col-0 under both carbon and nitrogen starvation (Figure S10b,c).

Notably, *vps9a-2* mutant exhibited a more sensitive phenotype than *atg7-2* under carbon starvation (Figure 4d), with significantly lower survival rates on the fifth day (Figure 4e). Under -N conditions, both *vps9a-2* and *atg7-2* displayed pronounced senescence compared to Col-0 (Figure 4f), but *vps9a-2* showed significantly lower chlorophyll content than *atg7-2* (Figure 4g).

ATG8-PE conjugate formation and its association with autophagosome membranes, is promoted by the ATG5-ATG12 complex. Analysis of ATG8-PE accumulation revealed that *vps9a-2* displayed levels comparable to those in Col-0, in contrast to the deficiencies detected in *atg7-2* and *atg5-1* (Figure 5a). Formation of the ATG5-ATG12 complex was also unaffected in the *vps9a-2* mutant under various nutrient conditions (Figure 5b).

To further understand how *VPS9a* participates in autophagy regulation in Arabidopsis, *vps9a-2* was crossed with the *35S:GFP-ATG8a* and autophagic flux was assessed

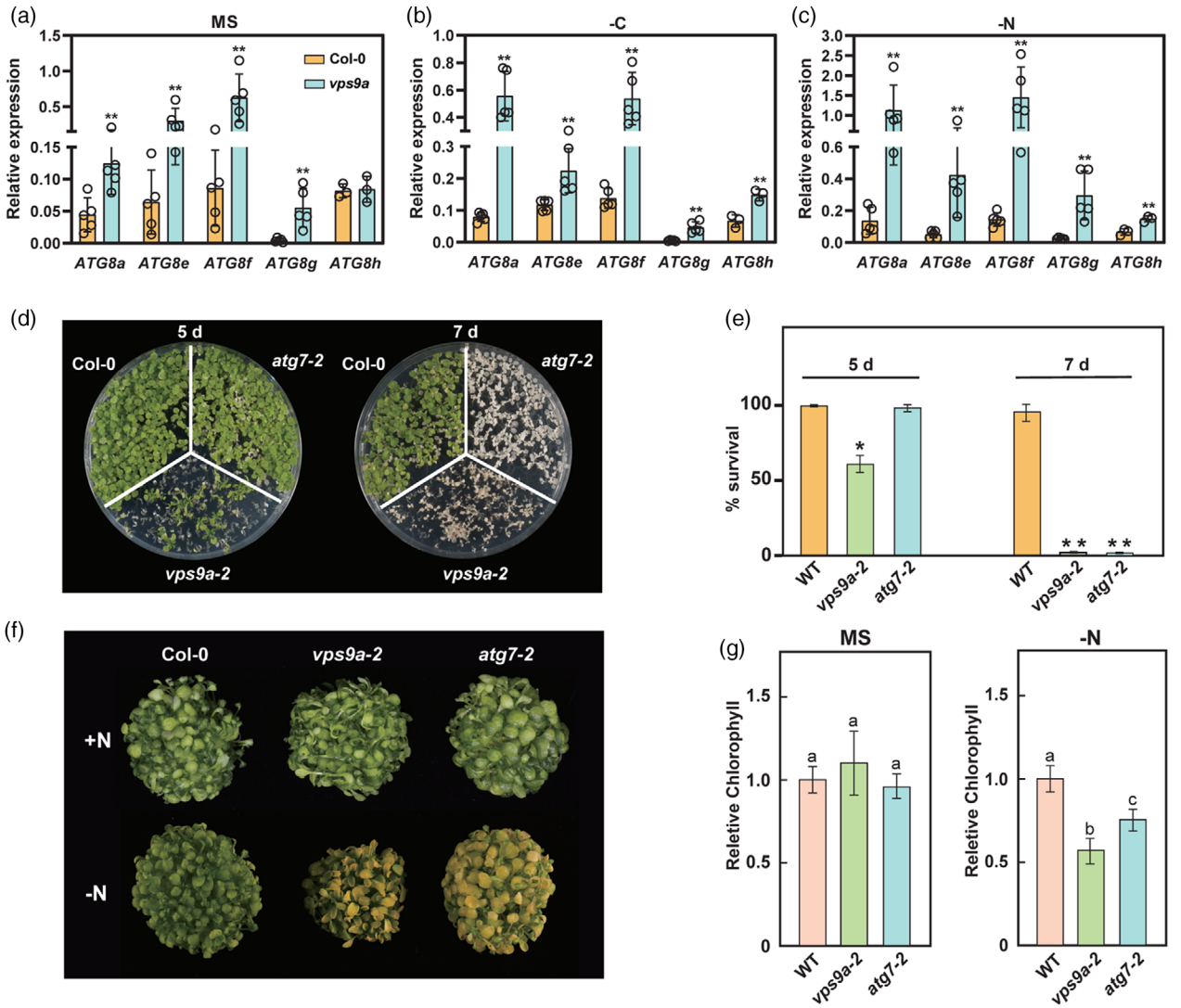

Figure 4. Relative expression levels of *ATG8* genes and phenotypic comparison of Col-0, *vps9a-2*, *atg7-2* seedlings under nutrient starvation.
(a–c) The transcription level of *ATG8a* (AT4G21980), *ATG8e* (AT2G45170), *ATG8f* (AT4G16520), *ATG8g* (AT3G60640), and *ATG8h* (AT3G06420) in Col-0 and *vps9a-2* under MS (a), carbon starvation (b) and nitrogen deprivation (c). Expression levels were measured using qRT-PCR and normalized with *Actin* (AT3G18780); relative expression of genes was calculated by the $2^{-\Delta CT}$ method. Data are presented as mean ± SD ($n \geq 3$). Asterisks indicate significant differences between *vps9a-2* and Col-0 (*$P < 0.05$; **$P < 0.01$; Student's *t*-test).
(d) The images show the survival and growth status of seedlings after the specified treatment periods.
(e) Survival rates of Col-0, *vps9a-2*, and *atg7-2* seedlings after 5 and 7 days of darkness. Data are presented as mean ± SD ($n = 3$). Asterisks indicate significant differences compared to WT (*$P < 0.05$; **$P < 0.01$; Student's *t*-test).
(f) Phenotypes of Col-0, *vps9a-2*, and *atg7-2* under nitrogen starvation (-N) conditions. Both *vps9a-2* and *atg7-2* showed pronounced senescence compared to Col-0.
(g) Relative chlorophyll content under nitrogen starvation. Data were normalized to the Col-0 and represented by mean ± SD ($n = 3$; *$P < 0.05$; **$P < 0.01$; Student's *t*-test).

by measuring free GFP accumulation over time under carbon starvation (-C). The *atg7* mutant showed severely impaired autophagic flux, whereas free GFP accumulated normally in both *vps9a-2* and Col-0 (Figure 5c). Additionally, we found that the mutation of *vps9a* led to a significant reduction in GFP-ATG8a protein levels (Figure 5c). Further, induction of *VPS9a* accumulation under nitrogen deprivation was also observed. Upon application of exogenous Concanamycin A (ConA), an inhibitor specific to V-ATPase, VPS9a-targeted components were accumulated in the central vacuole (Figure 5d).

The *GFP-ATG8a* reporter was used to monitor the accumulation of autophagic bodies in Col-0 and *vps9a-2* cells. Under -N and -C induction, the GFP-ATG8a targeted component accumulated in both Col-0 and *vps9a-2* cells (Figure 6a,b), whereas the loss of *vps9a* function led to a notable reduction within the central vacuole (Figure 6d). We also observed that *vps9a* led to a weakened GFP-

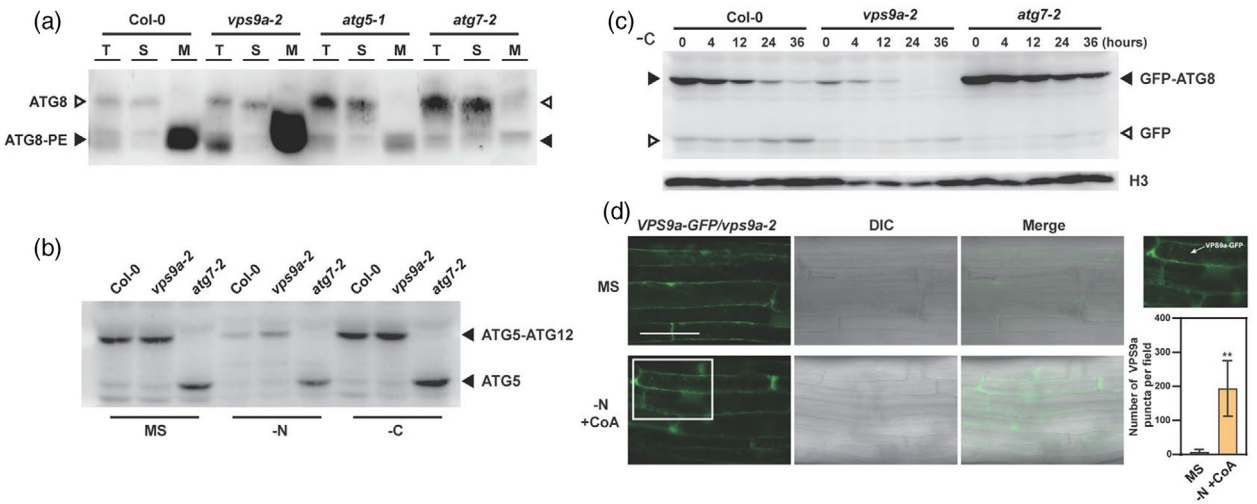

Figure 5. Accumulation of lipidated ATG8 in Col-0, *vps9a-2*, *atg5-1*, and *atg7-2*.
(a) The black arrow indicates the ATG8-PE specificity band. Soluble (S) and membrane (M) fractions were extracted from total extracts (TE). In the membrane fraction, Col-0 showed normal accumulation of ATG8-PE, and a similar result was observed in *vps9a-2*.
(b) *vps9a-2* accumulates ATG5-ATG12 conjugate normally. The upper arrow indicates the ATG5-ATG12 complex, while the lower part represents free ATG5. Samples were collected from 10-days-old seedlings, with -N and -C samples collected at 36 h post-treatment.
(c) Plants were grown under continuous light for 1 week, followed by dark treatment. Samples for carbon starvation were collected at the indicated time points to detect the accumulation of GFP-ATG8 and free GFP.
(d) Nitrogen starvation (-N) induces the accumulation of VPS9a. VPS9a puncta in the central vacuole were observed after 6 h of -N treatment, and the number of puncta was quantified under normal and -N conditions (n = 10, $*P < 0.05$; $**P < 0.01$; Student's t-test). Scale bar = 50 μm.

ATG8a signal (Figure 6c). This is consistent with the weaker GFP and GFP-ATG8a protein levels detected during autophagy flux analysis (Figure 5c). These results suggested a potential regulatory process leading to decreased GFP-ATG8a protein levels.

To determine whether *VPS9a* has similar effects on other ATG8 homologs, *35S:GFP-ATG8e* was crossed with the *vps9a-2*. The resulting accumulation of autophagic bodies marked by ATG8e was similar to that of GFP-ATG8a, further confirming the impact of *VPS9a* on autophagic body accumulation (Figure 6e,g). Under carbon starvation, a similar reduction (~50%) in the number of autophagic bodies was observed in the *vps9a-2* background (Figure 6e,g). However, GFP-ATG8e did not exhibit signal reduction similar to that of GFP-ATG8a (Figure 6f), indicating that *VPS9a* differentially regulates homologous ATG8 proteins.

DISCUSSION

VPS9a-mediated endosomal trafficking modulates the GS/GOGAT cycle response during plant adaptation to nutrient starvation

The endosomal sorting system is a fundamental pathway for intracellular transport in plants and plays a crucial role in nutrient distribution and metabolic regulation (Ivanov & Vert, 2021; Xue et al., 2024; Zhu et al., 2024). *VPS9a*, a key regulator of intracellular trafficking, mediates endosomal transport (Goh et al., 2007; Ito et al., 2018). In the present study, we showed that the loss of *VPS9a* function disrupts nitrogen metabolism in Arabidopsis (Figure 1). Specifically, during the low-nitrogen response, both GS and NADH-GOGAT exhibited increased activity (Figure 1e,f). Previous studies have shown that nitrogen starvation activates major degradation pathways, leading to the breakdown of proteins and organelles (del Mar Rubio-Wilhelmi et al., 2012; Gironde et al., 2015; Marshall & Vierstra, 2018) and results in NH_4^+ accumulation, thereby enhancing GS activity to assimilate inorganic nitrogen into organic forms (Barneix et al., 1984; Lemaitre et al., 2008). Our WGCNA and KEGG analyses revealed a strong correlation between key degradation pathways and GS/GOGAT activity, including the proteasome, autophagy, and endocytic pathways (Figures S5–S8). *VPS9a* regulates the expression of autophagy- and endocytic genes (Figure 2). The altered responses in the endosomal transport and degradation pathways in *vps9a-2* resulted in elevated GS and NADH-GOGAT activity and a notable response to nitrogen starvation.

Moreover, these disruptions in nitrogen remobilization were reflected in the levels of amino acids associated with the GS/GOGAT cycle. Notably, *vps9a-2* accumulated higher endogenous amino acid levels under normal conditions (0 h), indicating abnormal nitrogen metabolism caused by impaired endosomal trafficking (Figure 1g–i, Figure S1). This may result from the defective transport and metabolism of cargo components, leading to a feedback regulatory effect. Upon exposure to nitrogen deficiency, the

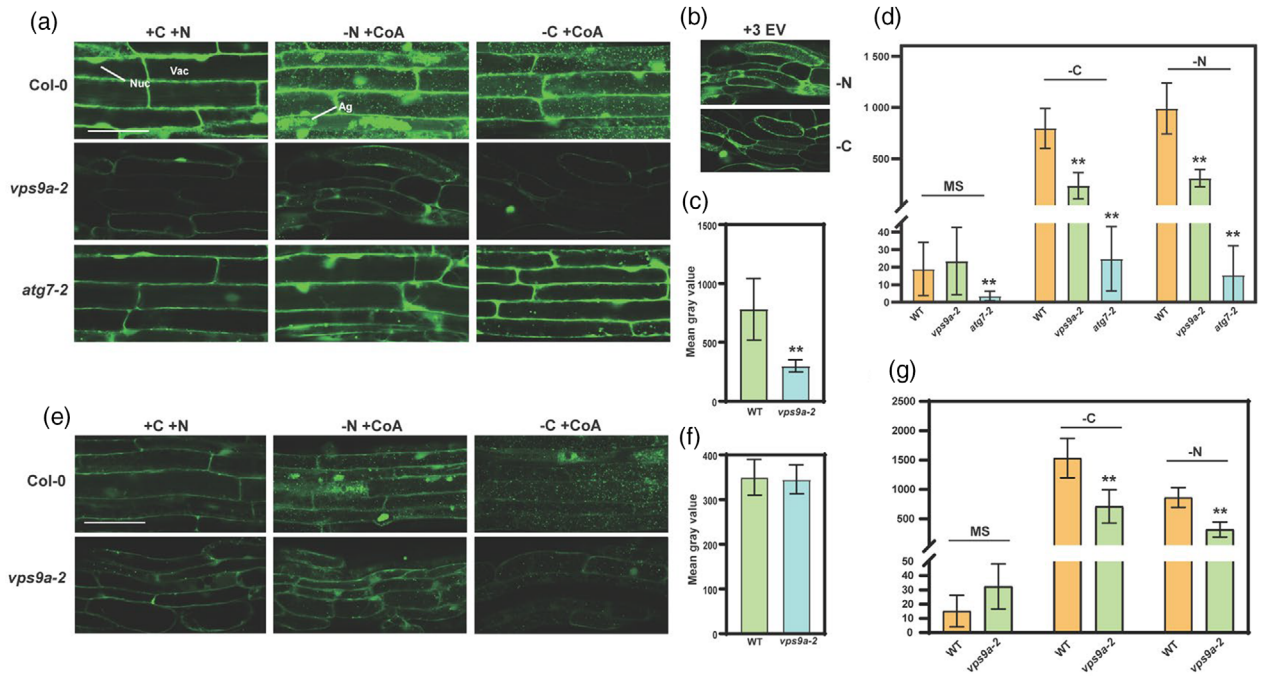

Figure 6. Lost function of *vps9a* results in less autophagic body accumulation.
(a) 7-days-old seedlings transferred to nitrogen-free (-N) liquid medium containing 1 μM Concanamycin A (ConA). After 4 h of treatment under light conditions, the accumulation of autophagic bodies was observed. For carbon starvation (-C) treatment, plants were incubated in the dark for 4 h. GFP-ATG8a signals in the roots were observed using confocal fluorescence microscopy. Each image was captured with the same parameters and magnification. Ag, autophagic body aggregates, Nuc, nucleus, Vac, vacuole. Scale bar = 50 μm.
(b) Images of *vps9a-2* from Figure 6a with brightness increased by +3 EV upon nitrogen or fixed-carbon starvation.
(c) Relative fluorescence intensity of *GFP-ATG8a* in WT and *vps9a-2* roots, signal intensity is represented by the average gray value of replicates ($n = 3$; $^*P < 0.05$; $^{**}P < 0.01$; Student's *t*-test).
(d) Quantification of autophagic bodies labeled by GFP-ATG8a. 200 × 200 μm area was captured for statistical analysis. Data are presented as mean ± SD ($n = 10$; $^*P < 0.05$; $^{**}P < 0.01$; Student's *t*-test).
(e) Observation of autophagosomes marked by GFP-ATG8e. Each image was captured with the same parameters. Scale bar = 50 μm.
(f) Relative fluorescence intensity of *GFP-ATG8e* in WT and *vps9a-2* roots, signal intensity is represented by the average gray value of replicates. ($n = 3$; $^*P < 0.05$; $^{**}P < 0.01$; Student's *t*-test).
(g) Quantification of autophagic bodies labeled by GFP-ATG8e in WT and *vps9a-2* roots. 200 × 200 μm area was captured for statistical analysis, presented by mean ± SD ($n = 8$; $^*P < 0.05$; $^{**}P < 0.01$; Student's *t*-test).

amino acid levels declined sharply, potentially contributing to the nitrogen starvation-sensitive phenotype of *vps9a-2*. Our findings provide physiological and metabolic insights into how the endosomal sorting pathway regulates plant responses to nutrient stress and how it plays a crucial role in regulating nitrogen remobilization during the GS/GOGAT-mediated starvation response in Arabidopsis.

Key components involved in endocytosis linking the GS/GOGAT-mediated nitrogen remobilization response to low-nitrogen

Within the endocytic interaction network, several key components of the ESCRT complex were identified as core regulators of this pathway (Figure 3d–f). Endocytosis is a critical mechanism for nutrient acquisition and environmental sensing in plants (Lou et al., 2020; Xia et al., 2020). Subcellular compartments are internalized via endocytosis, which relies on the ESCRT system for transport and sorting (Aniento et al., 2022; Gao et al., 2017). Recent studies have identified key regulatory components within the ESCRT system and other endosomal trafficking pathways (Reyes et al., 2011; Winter & Hauser, 2006). These subunits, along with other transport-related factors, participate in intracellular trafficking, autophagy, and multivesicular body (MVB) formation, which mediate the degradation of cellular components (Gao et al., 2015; Spitzer et al., 2015; Wang et al., 2017). Additionally, we identified several potential genes that may be involved in the endocytic pathway based on their high correlation with known endocytic genes in the interaction network. One notable gene, *ACA4*, which exhibited a high degree of expression in our network analysis, encoded a Ca^{2+}-ATPase pump localized to the vacuole (Figure 3d). ACA4 transports Ca^{2+} from the cytoplasm to other compartments (Li et al., 2023). The *aca4/aca11* double mutant exhibits elevated Ca^{2+} levels compared to wild-type plants, leading to the activation of salicylic acid signaling, a key regulator of plant senescence and programmed cell death (Boursiac et al., 2010). Another

potential regulatory gene identified in the endocytic pathway was *MKK2* (Figure 3d). Mitogen-activated protein kinase (MAPK) signaling pathways are involved in diverse plant processes, including growth, cold tolerance (Siodmak et al., 2023), oxidative stress adaptation, and immune responses such as pattern-triggered immunity (PTI) against biotic challenges (Takagi et al., 2019). These findings suggest that plants coordinate MAPK signaling and endocytosis in response to nitrogen starvation. Furthermore, we identified *TLP18.3* (Figure 3d), which has been implicated in photosystem II regulation (Jarvi et al., 2016). Given these findings, future research should explore the roles of photosynthesis, Ca^{2+} and MAPK signaling in endosomal trafficking and vacuolar transport, as well as their functional relevance in nitrogen metabolism. Understanding these pathways will provide deeper insight into the molecular mechanisms underlying nitrogen remobilization in plants.

The homologs of *ATG1* and *ATG8*, as core autophagy genes, regulate nitrogen recycling during starvation

Previous studies have shown that nitrogen deficiency affects the source-sink relationship in senescing tissues, with nitrogen remobilization regulated by autophagy-related genes (Di Berardino et al., 2018; Hollmann et al., 2014). During this process, targeted cytoplasmic components are translocated to the vacuole through the formation of autophagosomes (Lin et al., 2021; Nishimura & Tooze, 2020), which play a crucial role in supplying respiratory substrates under starvation conditions and help maintain energy balance in plants (Ferguson et al., 2021). Our results indicated that autophagy-related genes were significantly upregulated in response to nitrogen deficiency (Figure 2a–c). Additionally, in the autophagy interaction network, two *ATG8* genes (*ATG8a* and *ATG8b*) and two *ATG1* homologs (*ATG1a* and *ATG1b*) were identified as hub genes (Figure 3a–c). ATG1, which forms a complex with ATG13 and ATG101, is involved in the initiation of autophagy. The assembly of the ATG1 complex is promoted by changes in the external nutrient environment, and thus regulates AP formation by kinase activity (Li & Vierstra, 2014). The *atg1abc* triple mutant exhibits premature senescence under starvation (Qi et al., 2020). Another homologous autophagic protein, ATG8, has multiple homologs that specifically bind to adaptor proteins for recognizing and degrading substrates, including target proteins and organelles, such as chloroplasts and mitochondria (Li, Duckney, et al., 2022; Marshall & Vierstra, 2018). The modification and assembly of ATG8s are critical steps in the formation and maturation of AP (Johansen & Lamark, 2020). In both crops and Arabidopsis ATG8 and related pathways play a pivotal role in nitrogen remobilization. The *atg8a-i* nonuple mutant (Del Chiaro et al., 2024), along with other mutants related to ATG8 modification and assembly (e.g., *atg7*, *atg5*, *atg12*), exhibit hypersensitive phenotypes under nitrogen-deficient conditions (Chung et al., 2010; Fan et al., 2020; Thompson et al., 2005; Wada et al., 2015). Moreover, multiomics and ^{15}N labeling have demonstrated that defects in the ATG8-mediated autophagy pathway result in alterations in metabolism, lipid composition, and protein levels (Li et al., 2015; McLoughlin et al., 2018). During reproductive growth, impaired nitrogen remobilization disrupts the transfer of nitrogen from source tissues to reproductive organs and seeds, ultimately leading to reduced crop yield and quality (Chen et al., 2019; Erlichman et al., 2023; Fan et al., 2020). These findings emphasize the essential role of the ATG8-mediated autophagic pathway in regulating nutrient management under stress conditions, modulating the metabolism of aging tissues, and ensuring normal physiological processes during reproductive growth. In conclusion, based on our autophagy interaction network and the correlations observed in gene expression profiles, we propose that *ATG8* and *ATG1* serve as critical regulators of autophagy in *VPS9a*-mediated nitrogen remobilization in Arabidopsis.

The *VPS9a*-mediated endosomal sorting process affects autophagic body accumulation and modulates the levels of specific ATG8 homologs in Arabidopsis

Our results further confirm the role of *VPS9a* in autophagy. The lost function of *VPS9a* significantly inhibited autophagic body accumulation (Figure 6d,g), and under -C and -N conditions, *vps9a-2* exhibited a more sensitive phenotype than the autophagy mutant *atg7-2* (Figure 4d–g), which is consistent with previous reports on other components related to endosomal sorting pathways (Liu et al., 2018). This increased sensitivity may be attributed to the involvement of *VPS9a* in biological processes beyond autophagy, ultimately contributing to the observed carbon starvation phenotype. Additionally, *ATG8a* and other homologous genes were upregulated in response to starvation in the *vps9a-2* background, showing a significant increase compared to that of Col-0 (Figure 4b,c), which further confirmed that *VPS9a* affects the expression levels of core autophagy gene ATG8 homologs. This upregulation may reflect a compensatory response to dysfunction in endosomal trafficking pathways, leading to transport disruptions. This may require increased autophagic activity to maintain cellular homeostasis.

Furthermore, we investigated whether *VPS9a* regulates ATG8 lipidation. However, *VPS9a* did not affect the accumulation of ATG8-PE (Figure 5a) or ATG5-ATG12 complex formation (Figure 5b). Interestingly, *vps9a-2* influenced the protein levels of GFP-ATG8a, as revealed by western blotting (Figure 5c), which was further validated by observing the GFP-ATG8a signal intensity during autophagic body formation (Figure 6a,c). However, a similar effect was not observed

for GFP-ATG8e (Figure 6f). Previous studies have shown that ATG8a and ATG8e belong to different subclades of the ATG8 family. ATG8a, ATG8b, and ATG8c are classified into the same branch, whereas ATG8e shares a closer evolutionary relationship with ATG8f and ATG8g (Chen et al., 2024; Kellner et al., 2017). The current understanding of how endosomal sorting pathway components influence different ATG8 homologs remains limited. Recent studies suggested that FREE1 interacts with specific ATG8s and participates in AP closure (Zeng et al., 2023) indicating that ESCRT components may exhibit diverse functions in the regulation of ATG8 homologs. However, the biological functions and regulatory mechanisms underlying the differences among these ATG8 homologs remain poorly understood. Further research is warranted to elucidate the influence of endosomal sorting pathway components on ATG8a abundance. Specifically, it is essential to learn the regulatory roles of key endocytic hub genes that modulate the ATG8 homolog levels. This knowledge will contribute to a more comprehensive understanding of the mechanistic interplay between the endocytic and autophagic trafficking pathways in orchestrating nitrogen remobilization under nitrogen-limited conditions.

CONCLUSIONS

This study establishes *VPS9a* as a central regulator of nitrogen metabolism, autophagy, and endocytosis in Arabidopsis under nitrogen-deficient conditions. The loss of *VPS9a* function disrupts nitrogen remobilization, perturbs GS/GOGAT-associated regulatory networks, and leads to premature senescence. WGCNA revealed that *VPS9a* affects key modules associated with autophagy, endocytosis, and phosphatidylinositol signaling. Although *VPS9a* does not directly regulate the ATG8 conjugation system, it modulates the protein levels of ATG8a and the accumulation of autophagic bodies, indicating an indirect but pivotal role in autophagy.

Together, these findings revealed a previously uncharacterized mechanism linking membrane trafficking to nitrogen homeostasis. By positioning *VPS9a* at the intersection of endocytic and autophagic pathways, this study provides new insights into how plants coordinate nutrient recycling under stress.

MATERIALS AND METHODS

Plant materials

The *vps9a-2* (GABI_557C02), *atg7-2* (GABI_655B06) and *atg5-1* (SAIL_129_B07) mutants were previously described by Thompson et al. (2005), Goh et al. (2007), and Chung et al. (2010), and obtained from the Arabidopsis Biological Resource Center (ABRC, Ohio State University). These mutants were crossed with *GFP-ATG8a* and *GFP-ATG8e* to obtain homozygous lines.

To generate *35S:VPS9a-GFP/vps9a-2* lines, the full-length coding region of VPS9a was then amplified. The coding sequence of *VPS9a* was inserted into the linearized pEGAD vector (digested with AgeI) between the 35S promoter and the GFP tag using the ClonExpress II One Step Cloning Kit (Vazyme, Nanjing, China). The recombinant vector was then transformed into the *vps9a-2* background using *Agrobacterium*-mediated transformation and homozygous lines were obtained by multiple generations of self-crossing. Complementation lines (*VPS9apro:VPS9a-GFP/vps9a-2*) driven by the native *VPS9a* promoter were obtained from the Austrian Institute of Technology.

Plant phenotypic assays

Arabidopsis seeds were surface sterilized with 1% sodium hypochlorite. For carbon starvation (-C), seeds were sown on MS medium lacking sucrose, which contained 1% (w/v) agar and 2 mM MES-KOH, with the pH adjusted to 5.7 using KOH. Plants were placed at 4°C for 2 days to ensure consistent germination and then placed in a growth chamber under a 16-h light/8-h dark photoperiod at 22°C for 10 days. Subsequently, the seedlings were transferred to darkness for carbon starvation treatment. The seedlings were returned to normal conditions after 5 or 7 days of treatment. Survival rates were assessed after 1 week of recovery.

For nitrogen starvation (-N) experiments, seedlings were initially cultivated in liquid MS medium at 22°C under a 16-h light/ 8-h dark photoperiod for 7 days. The MS medium was then replaced with nitrogen-free MS medium, and the seedlings were maintained under these conditions for an additional week. The phenotypic characteristics of the various plant lines were documented using photographs.

Enzyme activity assay for the nitrogen metabolism pathway

Plant samples were collected after 0, 48, and 96-h nitrogen starvation (-N). Samples (0.1 g) were homogenized in 1 ml of Phosphate Buffer (pH 7.4) on ice. The homogenate was centrifuged at 14167 *g* for 10 min at 4°C, and the supernatant was collected and kept on ice for subsequent enzyme activity assays.

The activities of GS and GOGAT were measured using assay kits (Suzhou Grace Biotechnology Co., Ltd., China) according to the manufacturer's instructions.

Liquid chromatography-mass spectrometry (LC–MS/MS) analysis of amino acids

50 mg of plant tissue were transferred to a 1.5 ml centrifuge tube, followed by the addition of 300 μl methanol. The mixture was thoroughly vortexed and centrifuged at 22136 *g* rpm for 10 min at 4°C. The supernatant was collected for further analysis. For aspartate quantification, the supernatant was diluted 50-fold for LC–MS analysis. The supernatant was diluted 500-fold to detect the levels of glutamine, glutamate, arginine, and proline. The amino acid concentrations were determined using LC–MS under optimized conditions. Quantification was performed using standard calibration curves prepared from pure amino acid standards.

Transcriptome sequencing (RNA-seq) and data analysis

Leaf samples were collected after 0, 48, and 96-h nitrogen starvation (-N). Total RNA was extracted from each sample to prepare RNA libraries, which were sequenced using GENE DENOVO (Guangzhou, China). Gene expression levels were quantified as Transcripts Per Million (TPM).

Total RNA was extracted from each sample using a standardized protocol, and RNA quality and integrity were verified using an Agilent 2100 Bioanalyzer (Agilent, Santa Clara, CA, USA). RNA

libraries were prepared and sequenced by GENE DENOVO (Guangzhou, China) using the Illumina HiSeq2500™ system platform (Illumina, San Diego, CA, USA). Sequencing reads were aligned to the Arabidopsis reference genome, and gene expression levels were quantified as TPM to ensure comparability across samples. The Kyoto Encyclopedia of Genes and Genomes (KEGG) pathway enrichment analysis was then conducted to identify the metabolic and signaling pathways that were significantly enriched among the genes within each module.

Construction of co-expression network and KEGG enrichment analysis

Weighted gene co-expression network analysis (WGCNA) was performed using the OmicSmart platform (GENE DENOVO) (https://www.omicsmart.com). The correlation between the modules and physiological enzyme activity was analyzed based on previously described methods (Langfelder & Horvath, 2008). All raw data were filtered and low-expression and low-quality RNA-seq data were removed. Co-expression networks were constructed using the TPM values obtained from RNA-seq.

First, the pickSoftThreshold function was used to estimate the soft-threshold power, and an appropriate soft threshold was selected to construct the correlation matrix. In our analysis, the following parameters were used to construct the co-expression network: $\beta = 8$, minModuleSize = 50, and mergeCutHeight = 0.1.

Different modules were then used to construct a module-trait relationship heatmap to identify modules highly correlated with physiological traits under nitrogen starvation conditions ($^{*}P < 0.05$; $^{**}P < 0.01$). Genes from significantly correlated modules were subjected to enrichment analysis using the KEGG database, and KEGG pathway analysis was performed using KOBAS-i (http://kobas.cbi.pku.edu.cn/). Bubble plots displayed the top ten pathways.

Profile model analysis of autophagy and endocytosis-related genes

Profile model analysis of genes related to autophagy and endocytosis was conducted using the OmicShare platform (https://www.omicshare.com). The genes involved in the analysis were normalized using the $\log_2$ method, and significantly enriched trend modules were identified and displayed.

Identification of hub genes in key regulatory modules

The results of the WGCNA and KEGG analyses were used to identify modules significantly enriched for the autophagy and endocytic pathways. The top 10 000 weight values for gene correlations were extracted from the identified modules, and genes associated with autophagy and endocytosis in Col-0 (Table S7), *vps9a-2* (Table S8), and *35S:VPS9a-GFP/vps9a-2* (Table S9) were identified with high weight values. The interaction network based on these genes was constructed using the Cytoscape software v3.10.2 (Otasek et al., 2019), and the degree value for each gene within the network was calculated. Hub genes for the autophagy and endocytosis pathways were selected based on their degree values, as follows:

Col-0 autophagy: degree >50; Col-0 endocytosis: degree >14.

vps9a-2 autophagy: degree >5; *vps9a-2* endocytosis: degree >10.

35S:VPS9a-GFP/vps9a-2 autophagy: degree >3; *35S:VPS9a-GFP/vps9a-2* endocytosis: degree >18.

Immunoblot assay

To detect GFP and ATG5, total extracts were prepared from 200 mg of seedlings. After grinding, samples were mixed with sample buffer (100 mM Tris–HCl, 4% SDS, 0.2% bromophenol blue, and 20% glycerol), heated to 98°C for 8 min, and centrifuged at 19283 *g* for 10 min. The supernatants were separated on a 10% acrylamide gel. The antibodies used for western blotting included ATG5 (Thompson et al., 2005) histone H3 (ab1791, 1:10 000 dilution), anti-GFP (ab183734, 1:10 000 dilution), and a secondary antibody (IgG-HRP, ab6721, 1:5000 dilution) obtained from Abcam (Cambridge, UK). The blots were visualized using a Tanon 5200 Chemiluminescent Analyzer (Tanon, Shanghai, China).

For the detection of ATG8 and PE conjugates, membrane fractions were collected from total seedling extracts by centrifugation at 100 000 g for 10 min at 4°C. The pellet was resuspended in TNPI buffer (50 mM Tris–HCl, pH 8.0, 150 mM NaCl, 1 mM PMSF, and 10 mM iodoacetamide) containing 0.5% (v/v) Triton X-100 (Liu et al., 2020). After clarification, the samples were subjected to SDS-PAGE in the presence of 6 M urea and immunoblotted with an anti-ATG8 antibody (Chung et al., 2010).

Confocal fluorescence microscopy and image analysis

Fluorescent images were captured using a confocal microscope (FV3000; Olympus, Tokyo, Japan). GFP signals were detected using a 488 nm laser combined with a 500–550 nm filter. The images were processed and converted to TIFF files using the FV31S-SW (Olympus, Ver 2.6) software.

To quantify the accumulation of autophagic bodies in the central vacuole area of roots, we used ImageJ (Schneider et al., 2012) to count the number of autophagic bodies within a 200 × 200 μm field of view. The intensity of the fluorescence signal, represented by the mean gray value of each image, was used to evaluate the GFP signal intensity in different lines. The photos used for statistical analysis were captured using the same parameters, and the original files of the images were measured using CellSens Dimension v4.2.1 (Olympus) software.

qRT-PCR analysis

Fresh samples were collected from each group (three biological replicates) and immediately flash frozen in liquid nitrogen. Total RNA was extracted using a FastPure Plant Total RNA Isolation Kit (Vazyme). cDNA was synthesized using HiScript III RT SuperMix (Vazyme), according to the manufacturer's protocol. The qPCR reactions were set up using ChamQ Universal SYBR qPCR Master Mix (Vazyme) and performed on a CFX Connect PCR System (Bio-Rad, Hercules, CA, USA). Gene expression levels were quantified and determined using the $2^{-\Delta Ct}$ method; primers used for analysis are shown in Table S1.

Chlorophyll content measurement

Fresh plant samples (0.2 g) were homogenized in 10 ml ethanol and centrifuged at 9838 *g* for 10 min. The supernatant was collected, and the volume was adjusted to 50 ml with 95% ethanol and mixed thoroughly. The absorbance of the pigment extract was measured at 665 nm and 649 nm according to a previously described method (Liang et al., 2017). All samples were normalized to Col-0.

AUTHOR CONTRIBUTIONS

The authors confirm their contributions: BY, YZ, YS, SW, QP, and CY collaborated in sample collection, validation

experiments, and data analysis. WH, YW, and FL designed the experiments. BY completed the preparation of the original draft and writing, and WH, YW, and FL revised and reviewed the manuscript, The -C phenotyping of *VPS9apro:VPS9a-GFP/ vps9a-2* line was carried out in TR's lab under his guidance. All the authors have read and agreed to the final version of the manuscript.

ACKNOWLEDGEMENTS

We thank Dr. Wang Qi for his support and assistance during the experiments, and Professor Eva Benková (Institute of Science and Technology Austria) for kindly providing the *VPS9apro:VPS9a-GFP/vps9a-2* complementation line. This work was supported by grants from the Double Thousand Plan of Jiangxi Province (jxsq2023201126 to Fen Liu), International Science and Technology Cooperation Project of Jiangxi Province (20232BBH80003 to Fen Liu), and Xuncheng Talent Program (JJXC2023053 to Fen Liu).

CONFLICTS OF INTEREST

The authors declare no conflicts of interest.

DATA AVAILABILITY STATEMENT

The data presented in this study are available upon request from the corresponding author. Transcriptomic data were deposited in the National Center for Bioinformation (https://www.cncb.ac.cn) under the accession number PRJCA033254.

SUPPORTING INFORMATION

Additional Supporting Information may be found in the online version of this article.

Figure S1. Validation of -C phenotypes in Col-0, *VPS9apro:VPS9a-GFP/vps9a-2*, and the *vps9a-2*. (a) Phenotypes of 7-day-old Arabidopsis seedlings (Col-0, *vps9a-2*, and *VPS9apro:VPS9a-GFP/vps9a-2*) complementation line after 5 days of carbon starvation (-C). (b) Quantification of survival rates under -C conditions (**$P < 0.01$, Student's *t*-test). (c) Enlarged images showing seedling morphology under -C treatment.

Figure S2. Schematic representation of the GS/GOGAT cycle and endogenous Arg and Pro contents. (a) Profiling of key nitrogen metabolites of GS/GOGAT cycle. Aspartate (Asp), Proline (Pro), Glutamine (Gln), Glutamate (Glu), 2-oxoglutarate (2-OG), Arginine (Arg). (b) Arg content. (C) Pro content ($n = 6$, $P < 0.05$, Student's *t*-test).

Figure S3. Principal component analysis and division of modules by the Dynamic Tree Cut method. (a) Principal component analysis (PCA) of the RNA-seq data. (b) Dendrogram represents the hierarchical clustering of gene expression profiles in Col-0. The bottom panel shows the dynamic tree cut and merged dynamic module colors, indicating different clusters of co-expressed genes. (c) Hierarchical clustering of gene expression profiles in *vps9a-2*. The bottom panel shows the dynamic tree cut and merged dynamic module colors, indicating different clusters of co-expressed genes. (d) Hierarchical clustering of gene expression profiles in *35S:VPS9a-GFP/vps9a-2*. The bottom panel shows the dynamic tree cut and merged dynamic module colors, indicating different clusters of co-expressed genes.

Figure S4. Soft power curve used for WGCNA analysis. (a) Col-0, (b) *vps9a-2*, and (c) *35S:VPS9a-GFP/vps9a-2*. Left panel scale shows the scale-free topology model fit index (y-axis) as a function of the soft-thresholding power (x-axis). The red horizontal line indicates the threshold for a scale-free topology model fit index of 0.90 and right panels show the result of mean connectivity analysis, and the decrease in mean connectivity is observed with increasing soft-thresholding power.

Figure S5. Module identification in WGCNA and the number of genes in each module. (a) Col-0, (b) *vps9a-2*, and (c) *35S:VPS9a-GFP/vps9a-2*. Plots display the number of genes in each module identified by WGCNA. Each bar is color-coded to represent a specific module.

Figure S6. Identification of key modules in the GS/GOGAT cycle. (a–c) Correlations of GS activity and NADH-GOGAT activity with WGCNA modules of Col-0 (a), *35S:VPS9a-GFP/vps9a-2* (b), and *vps9a-2* (c) (*$P < 0.05$; **$P < 0.01$).

Figure S7. KEGG enrichment analysis of key modules in Col-0. The plots display enriched KEGG terms for key modules, showing the gene ratio (x-axis) and number of genes associated with each term (dot size). The color gradient represents $-\log_{10}$ (*P*-value), indicating the significance of enrichment, and shows the top 10 enriched KEGG pathways for each module.

Figure S8. KEGG enrichment analysis of key modules in *35S:VPS9a-GFP/vps9a-2*. The plots display enriched KEGG terms for key modules, showing the gene ratio (x-axis) and number of genes associated with each term (dot size). The color gradient represents $-\log_{10}$ (*P*-value), indicating the significance of enrichment, and shows the top 10 enriched KEGG pathways for each module.

Figure S9. KEGG enrichment analysis of key modules in *vps9a-2*. The plots display enriched KEGG terms for key modules, showing the gene ratio (x-axis) and number of genes associated with each term (dot size). The color gradient represents $-\log_{10}$ (*P*-value), indicating the significance of enrichment, and shows the top 10 enriched KEGG pathways for each module.

Figure S10. Relative expression levels of *ATG2*, *ATG6*, *ATG7* under fixed-carbon starvation. Expression levels were measured using qRT-PCR and normalized with *actin* (AT3G18780), relative expression of genes were calculated by $2^{-\Delta CT}$ method. (a) Gene expression levels under MS conditions. (b) Expression of *ATG2*, *ATG6*, and *ATG7* under -C conditions. Data are presented as mean ± SD ($n = 3$). Asterisks indicate significant differences between *vps9a-2* and Col-0 (*$P < 0.05$, **$P < 0.01$; Student's *t*-test), (c) Expression of *ATG2*, *ATG6*, and *ATG7* under -N conditions. Data are presented as mean ± SD ($n = 3$). Asterisks indicate significant differences between *vps9a-2* and Col-0 (*$P < 0.05$, **$P < 0.01$, Student's *t*-test).

Figure S11. Original images of the western blot.

Table S1. Primers used in this study.

Table S2. Gene expression profiles used for WGCNA analysis in Col-0.

Table S3. Gene expression profiles used for WGCNA analysis in *vps9a-2*.

Table S4. Gene expression profiles used for WGCNA analysis in *35S:VPS9a-GFP/vps9a-2*.

Table S5. Autophagy-related gene expression profiles used for trend analysis.

Table S6. Endocytosis-related gene expression profiles used for trend analysis.

Table S7. The correlation of autophagy-related genes for constructing an interaction network in Col-0.

Table S8. The correlation of endocytosis-related genes for constructing an interaction network in Col-0.

Table S9. The correlation of autophagy-related genes for constructing an interaction network in *vps9a-2*.

Table S10. The correlation of endocytosis-related genes for constructing an interaction network in *vps9a-2*.

Table S11. The correlation of autophagy-related genes for constructing an interaction network in *35S:VPS9a-GFP/vps9a-2*.

Table S12. The correlation of endocytosis-related genes for constructing an interaction network in *35S:VPS9a-GFP/vps9a-2*.

REFERENCES

Aniento, F., **de Medina, S.**, **Hernandez, V.**, **Dagdas, Y.**, **Rojas-Pierce, M.** & **Russinova, E.** (2022) Molecular mechanisms of endomembrane trafficking in plants. *Plant Cell*, **34**, 146–173.

Balotf, S., **Kavoosi, G.** & **Kholdebarin, B.** (2016) Nitrate reductase, nitrite reductase, glutamine synthetase, and glutamate synthase expression and activity in response to different nitrogen sources in nitrogen-starved wheat seedlings. *Biotechnology and Applied Biochemistry*, **63**, 220–229.

Baral, A., **Irani, N.G.**, **Fujimoto, M.**, **Nakano, A.**, **Mayor, S.** & **Mathew, M.K.** (2015) Salt-induced remodeling of spatially restricted clathrin-independent endocytic pathways in Arabidopsis root. *Plant Cell*, **27**, 1297–1315.

Barneix, A.J., **James, D.M.**, **Watson, E.F.** & **Hewitt, E.J.** (1984) Some effects of nitrate abundance and starvation on metabolism and accumulation of nitrogen in barley (*Hordeum vulgare* L. cv Sonja). *Planta*, **162**, 469–476.

Boura, E., **Rozycki, B.**, **Herrick, D.Z.**, **Chung, H.S.**, **Vecer, J.**, **Eaton, W.A.** ***et al.*** (2011) Solution structure of the ESCRT-I complex by small-angle X-ray scattering, EPR, and FRET spectroscopy. *Proceedings of the National Academy of Sciences of the United States of America*, **108**, 9437–9442.

Boursiac, Y., **Lee, S.M.**, **Romanowsky, S.**, **Blank, R.**, **Sladek, C.**, **Chung, W.S.** ***et al.*** (2010) Disruption of the vacuolar calcium-ATPases in Arabidopsis results in the activation of a salicylic acid-dependent programmed cell death pathway. *Plant Physiology*, **154**, 1158–1171.

Buser, D.P. & **Spang, A.** (2023) Protein sorting from endosomes to the TGN. *Frontiers in Cell and Development Biology*, **11**, 1140605.

Cao, J., **Zheng, X.**, **Xie, D.**, **Zhou, H.**, **Shao, S.** & **Zhou, J.** (2022) Autophagic pathway contributes to low-nitrogen tolerance by optimizing nitrogen uptake and utilization in tomato. *Horticulture Research*, **9**, uhac068.

Cardona-Lopez, X., **Cuyas, L.**, **Marin, E.**, **Rajulu, C.**, **Irigoyen, M.L.**, **Gil, E.** ***et al.*** (2015) ESCRT-III-associated protein ALIX mediates high-affinity phosphate transporter trafficking to maintain phosphate homeostasis in Arabidopsis. *Plant Cell*, **27**, 2560–2581.

Chen, Q., **Soulay, F.**, **Saudemont, B.**, **Elmayan, T.**, **Marmagne, A.** & **Masclaux-Daubresse, C.L.** (2019) Overexpression of ATG8 in Arabidopsis stimulates autophagic activity and increases nitrogen remobilization efficiency and grain filling. *Plant and Cell Physiology*, **60**, 343–352.

Chen, X., **He, Y.**, **Wu, Z.**, **Lu, X.**, **Yin, Z.**, **Zhao, L.** ***et al.*** (2024) Systematic analysis and expression of Gossypium ATG8 family reveals the roles of GhATG8f responding to salt stress in cotton. *Plant Cell Reports*, **43**, 58.

Chung, T., **Phillips, A.R.** & **Vierstra, R.D.** (2010) ATG8 lipidation and ATG8-mediated autophagy in Arabidopsis require ATG12 expressed from the differentially controlled ATG12A AND ATG12B loci. *The Plant Journal*, **62**, 483–493.

Chung, T., **Suttangkakul, A.** & **Vierstra, R.D.** (2009) The ATG autophagic conjugation system in maize: ATG transcripts and abundance of the ATG8-lipid adduct are regulated by development and nutrient availability. *Plant Physiology*, **149**, 220–234.

Cruz, J.L., **Mosquim, P.R.**, **Pelacani, C.R.**, **Araújo, W.L.** & **DaMatta, F.M.** (2004) Effects of nitrate nutrition on nitrogen metabolism in cassava. *Biologia Plantarum*, **48**, 67–72.

Del Chiaro, A., **Grujic, N.**, **Zhao, J.**, **Papareddy, R.K.**, **Gao, P.**, **Ma, J.** ***et al.*** (2024) Nonuple atg8 mutant provides genetic evidence for functional specialization of ATG8 isoforms in *Arabidopsis thaliana*. Preprint at bioRxiv.

del Mar Rubio-Wilhelmi, M., **Sanchez-Rodriguez, E.**, **Rosales, M.A.**, **Blasco, B.**, **Rios, J.J.**, **Romero, L.** ***et al.*** (2012) Ammonium formation and assimilation in P(SARK)colon, two colonsIPT tobacco transgenic plants under low N. *Journal of Plant Physiology*, **169**, 157–162.

Di Berardino, J., **Marmagne, A.**, **Berger, A.**, **Yoshimoto, K.**, **Cueff, G.**, **Chardon, F.** ***et al.*** (2018) Autophagy controls resource allocation and protein storage accumulation in Arabidopsis seeds. *Journal of Experimental Botany*, **69**, 1403–1414.

Ebine, K., **Fujimoto, M.**, **Okatani, Y.**, **Nishiyama, T.**, **Goh, T.**, **Ito, E.** ***et al.*** (2011) A membrane trafficking pathway regulated by the plant-specific RAB GTPase ARA6. *Nature Cell Biology*, **13**, 853–859.

Ekanayake, G., **Smith, J.M.**, **Jones, K.B.**, **Stiers, H.M.**, **Robinson, S.J.**, **LaMontagne, E.D.** ***et al.*** (2021) DYNAMIN-RELATED PROTEIN DRP1A functions with DRP2B in plant growth, flg22-immune responses, and endocytosis. *Plant Physiology*, **185**, 1986–2002.

Erlichman, O.A., **Weiss, S.**, **Abu Arkia, M.**, **Ankary-Khaner, M.**, **Soroka, Y.**, **Jasinska, W.** ***et al.*** (2023) Autophagy in maternal tissues contributes to Arabidopsis seed development. *Plant Physiology*, **193**, 611–626.

Fan, T., **Yang, W.**, **Zeng, X.**, **Xu, X.**, **Xu, Y.**, **Fan, X.** ***et al.*** (2020) A Rice autophagy gene OsATG8b is involved in nitrogen remobilization and control of grain quality. *Frontiers in Plant Science*, **11**, 588.

Ferguson, J.N., **Tidy, A.C.**, **Murchie, E.H.** & **Wilson, Z.A.** (2021) The potential of resilient carbon dynamics for stabilizing crop reproductive development and productivity during heat stress. *Plant, Cell & Environment*, **44**, 2066–2089.

Gan, P., **Luo, X.**, **Wei, H.**, **Hu, Y.**, **Li, R.** & **Luo, J.** (2023) Identification of hub genes that variate the qCSS12-mediated cold tolerance between indica and japonica rice using WGCNA. *Plant Cell Reports*, **43**, 24.

Gao, C., **Luo, M.**, **Zhao, Q.**, **Yang, R.**, **Cui, Y.**, **Zeng, Y.** ***et al.*** (2014) A unique plant ESCRT component, FREE1, regulates multivesicular body protein sorting and plant growth. *Current Biology*, **24**, 2556–2563.

Gao, C., **Zhuang, X.**, **Cui, Y.**, **Fu, X.**, **He, Y.**, **Zhao, Q.** ***et al.*** (2015) Dual roles of an Arabidopsis ESCRT component FREE1 in regulating vacuolar protein transport and autophagic degradation. *Proceedings of the National Academy of Sciences of the United States of America*, **112**, 1886–1891.

Gao, C., **Zhuang, X.**, **Shen, J.** & **Jiang, L.** (2017) Plant ESCRT complexes: moving beyond endosomal sorting. *Trends in Plant Science*, **22**, 986–998.

Gironde, A., **Etienne, P.**, **Trouverie, J.**, **Bouchereau, A.**, **Le Caherec, F.**, **Leport, L.** ***et al.*** (2015) The contrasting N management of two oilseed rape genotypes reveals the mechanisms of proteolysis associated with leaf N remobilization and the respective contributions of leaves and stems to N storage and remobilization during seed filling. *BMC Plant Biology*, **15**, 59.

Gnyliukh, N., **Johnson, A.**, **Nagel, M.K.**, **Monzer, A.**, **Babic, D.**, **Hlavata, A.** ***et al.*** (2024) Role of the dynamin-related protein 2 family and SH3P2 in clathrin-mediated endocytosis in *Arabidopsis thaliana*. *Journal of Cell Science*, **137**, 8.

Goh, T., **Uchida, W.**, **Arakawa, S.**, **Ito, E.**, **Dainobu, T.**, **Ebine, K.** ***et al.*** (2007) VPS9a, the common activator for two distinct types of Rab5 GTPases, is essential for the development of Arabidopsis thaliana. *Plant Cell*, **19**, 3504–3515.

Hao, G.J., **Ying, J.**, **Li, L.S.**, **Yu, F.**, **Dun, S.S.**, **Su, L.Y.** ***et al.*** (2024) Two functionally interchangeable Vps9 isoforms mediate pollen tube penetration of style. *The New Phytologist*, **244**, 840–854.

Hargrove-Grimes, P., **Mondal, A.K.**, **Gumerson, J.**, **Nellissery, J.**, **Aponte, A.M.**, **Gieser, L.** ***et al.*** (2020) Loss of endocytosis-associated RabGEF1 causes aberrant morphogenesis and altered autophagy in photoreceptors leading to retinal degeneration. *PLoS Genetics*, **16**, e1009259.

He, Y., **Gao, J.**, **Luo, M.**, **Gao, C.**, **Lin, Y.**, **Wong, H.Y.** ***et al.*** (2023) VAMP724 and VAMP726 are involved in autophagosome formation in Arabidopsis thaliana. *Autophagy*, **19**, 1406–1423.

Henne, W.M., **Buchkovich, N.J.** & **Emr, S.D.** (2011) The ESCRT pathway. *Developmental Cell*, **21**, 77–91.

Hilleary, R., **Paez-Valencia, J.**, **Vens, C.S.**, **Toyota, M.**, **Palmgren, M.** & **Gilroy, S.** (2020) Tonoplast-localized Ca(2+) pumps regulate Ca(2+) signals during pattern-triggered immunity in Arabidopsis thaliana. *Proceedings of the National Academy of Sciences of the United States of America*, **117**, 18849–18857.

Hilscher, J., **Kapusi, E.**, **Stoger, E.** & **Ibl, V.** (2016) Cell layer-specific distribution of transiently expressed barley ESCRT-III component HvVPS60 in developing barley endosperm. *Protoplasma*, **253**, 137–153.

Hodges, M. (2002) Enzyme redundancy and the importance of 2-oxoglutarate in plant ammonium assimilation. *Journal of Experimental Botany*, **53**, 905–916.

Hollmann, J., **Gregersen, P.L.** & **Krupinska, K.** (2014) Identification of predominant genes involved in regulation and execution of senescence-associated nitrogen remobilization in flag leaves of field grown barley. *Journal of Experimental Botany*, **65**, 3963–3973.

Ibl, V., **Csaszar, E.**, **Schlager, N.**, **Neubert, S.**, **Spitzer, C.** & **Hauser, M.T.** (2012) Interactome of the plant-specific ESCRT-III component AtVPS2.2 in *Arabidopsis thaliana*. *Journal of Proteome Research*, **11**, 397–411.

Isono, E. (2021) ESCRT is a great sealer: non-endosomal function of the ESCRT machinery in membrane repair and autophagy. *Plant & Cell Physiology*, **62**, 766–774.

Ito, E., **Ebine, K.**, **Choi, S.W.**, **Ichinose, S.**, **Uemura, T.**, **Nakano, A.** ***et al.*** (2018) Integration of two RAB5 groups during endosomal transport in plants. *eLife*, **7**, e34064.

Ivanov, R. & **Vert, G.** (2021) Endocytosis in plants: peculiarities and roles in the regulated trafficking of plant metal transporters. *Biology of the Cell*, **113**, 1–13.

Izumi, M., **Wada, S.**, **Makino, A.** & **Ishida, H.** (2010) The autophagic degradation of chloroplasts via rubisco-containing bodies is specifically linked to leaf carbon status but not nitrogen status in Arabidopsis. *Plant Physiology*, **154**, 1196–1209.

Jarvi, S., **Isojarvi, J.**, **Kangasjarvi, S.**, **Salojarvi, J.**, **Mamedov, F.**, **Suorsa, M.** ***et al.*** (2016) Photosystem II repair and plant immunity: lessons learned from Arabidopsis mutant lacking the THYLAKOID LUMEN PROTEIN 18.3. *Frontiers in Plant Science*, **7**, 405.

Javed, R., **Jain, A.**, **Duque, T.**, **Hendrix, E.**, **Paddar, M.A.**, **Khan, S.** ***et al.*** (2023) Mammalian ATG8 proteins maintain autophagosomal membrane integrity through ESCRTs. *The EMBO Journal*, **42**, e112845.

Jha, S.G. & **Larson, E.R.** (2023) Diversity of retromer-mediated vesicular trafficking pathways in plants. *Frontiers in Plant Science*, **14**, 1184047.

Johansen, T. & **Lamark, T.** (2020) Selective autophagy: ATG8 family proteins, LIR motifs and cargo receptors. *Journal of Molecular Biology*, **432**, 80–103.

Kellner, R., **De la Concepcion, J.C.**, **Maqbool, A.**, **Kamoun, S.** & **Dagdas, Y.F.** (2017) ATG8 expansion: a driver of selective autophagy diversification? *Trends in Plant Science*, **22**, 204–214.

Kovácik, J., **Repcák, M.** & **Kron, I.** (2006) Nitrogen deficiency induced changes of free amino acids and coumarin contents in the leaves of. *Acta Physiologiae Plantarum*, **28**, 159–164.

Krapp, A. (2015) Plant nitrogen assimilation and its regulation: a complex puzzle with missing pieces. *Current Opinion in Plant Biology*, **25**, 115–122.

Kurusu, T., **Koyano, T.**, **Hanamata, S.**, **Kubo, T.**, **Noguchi, Y.**, **Yagi, C.** ***et al.*** (2014) OsATG7 is required for autophagy-dependent lipid metabolism in rice postmeiotic anther development. *Autophagy*, **10**, 878–888.

Langfelder, P. & **Horvath, S.** (2008) WGCNA: an R package for weighted correlation network analysis. *BMC Bioinformatics*, **9**, 559.

Lee, Y., **Bak, G.**, **Choi, Y.**, **Chuang, W.I.**, **Cho, H.T.** & **Lee, Y.** (2008) Roles of phosphatidylinositol 3-kinase in root hair growth. *Plant Physiology*, **147**, 624–635.

Lemaitre, T., **Gaufichon, L.**, **Boutet-Mercey, S.**, **Christ, A.** & **Masclaux-Daubresse, C.** (2008) Enzymatic and metabolic diagnostic of nitrogen deficiency in *Arabidopsis thaliana* Wassileskija accession. *Plant & Cell Physiology*, **49**, 1056–1065.

Leprince, A.S., **Magalhaes, N.**, **De Vos, D.**, **Bordenave, M.**, **Crilat, E.**, **Clement, G.** ***et al.*** (2014) Involvement of phosphatidylinositol 3-kinase in the regulation of proline catabolism in *Arabidopsis thaliana*. *Frontiers in Plant Science*, **5**, 772.

Li, C., **Duckney, P.**, **Zhang, T.**, **Fu, Y.**, **Li, X.**, **Kroon, J.** ***et al.*** (2022) TraB family proteins are components of ER-mitochondrial contact sites and regulate ER-mitochondrial interactions and mitophagy. *Nature Communications*, **13**, 5658.

Li, F., **Chung, T.**, **Pennington, J.G.**, **Federico, M.L.**, **Kaeppler, H.F.**, **Kaeppler, S.M.** ***et al.*** (2015) Autophagic recycling plays a central role in maize nitrogen remobilization. *Plant Cell*, **27**, 1389–1408.

Li, F. & **Vierstra, R.D.** (2012) Autophagy: a multifaceted intracellular system for bulk and selective recycling. *Trends in Plant Science*, **17**, 526–537.

Li, F. & **Vierstra, R.D.** (2014) Arabidopsis ATG11, a scaffold that links the ATG1-ATG13 kinase complex to general autophagy and selective mitophagy. *Autophagy*, **10**, 1466–1467.

Li, H., **Nian, J.**, **Fang, S.**, **Guo, M.**, **Huang, X.**, **Zhang, F.** ***et al.*** (2022) Regulation of nitrogen starvation responses by the alarmone (p)ppGpp in rice. *Journal of Genetics and Genomics*, **49**, 469–480.

Li, W., **Wu, Z.** & **Liang, Y.** (2019) Vrl1 relies on its VPS9-domain to play a role in autophagy in Saccharomyces cerevisiae. *Cell Biology International*, **43**, 875–889.

Li, Z., **Harper, J.F.**, **Weigand, C.** & **Hua, J.** (2023) Resting cytosol Ca^{2+} level maintained by Ca^{2+} pumps affects environmental responses in Arabidopsis. *Plant Physiology*, **191**, 2534–2550.

Liang, Y., **Urano, D.**, **Liao, K.L.**, **Hedrick, T.L.**, **Gao, Y.** & **Jones, A.M.** (2017) A nondestructive method to estimate the chlorophyll content of Arabidopsis seedlings. *Plant Methods*, **13**, 26.

Liao, C.Y. & **Bassham, D.C.** (2020) Combating stress: the interplay between hormone signaling and autophagy in plants. *Journal of Experimental Botany*, **71**, 1723–1733.

Lin, Y., **Zeng, Y.**, **Zhu, Y.**, **Shen, J.**, **Ye, H.** & **Jiang, L.** (2021) Plant rho GTPase signaling promotes autophagy. *Molecular Plant*, **14**, 905–920.

Liu, F., **Hu, W.**, **Li, F.**, **Marshall, R.S.**, **Zarza, X.**, **Munnik, T.** ***et al.*** (2020) AUTOPHAGY-RELATED14 and its associated phosphatidylinositol 3-kinase complex promote autophagy in Arabidopsis. *Plant Cell*, **32**, 3939–3960.

Liu, F., **Hu, W.** & **Vierstra, R.D.** (2018) The vacuolar protein Sorting-38 subunit of the Arabidopsis Phosphatidylinositol-3-kinase complex plays critical roles in autophagy, endosome sorting, and gravitropism. *Frontiers in Plant Science*, **9**, 781.

Liu, X., **Hu, B.** & **Chu, C.** (2022) Nitrogen assimilation in plants: current status and future prospects. *Journal of Genetics and Genomics*, **49**, 394–404.

Lou, L., **Yu, F.**, **Tian, M.**, **Liu, G.**, **Wu, Y.**, **Wu, Y.** ***et al.*** (2020) ESCRT-I component VPS23A sustains salt tolerance by strengthening the SOS module in Arabidopsis. *Molecular Plant*, **13**, 1134–1148.

Marshall, R.S. & **Vierstra, R.D.** (2018) Autophagy: The master of bulk and selective recycling. *Annual Review of Plant Biology*, **69**, 173–208.

Masclaux-Daubresse, C., **Daniel-Vedele, F.**, **Dechorgnat, J.**, **Chardon, F.**, **Gaufichon, L.** & **Suzuki, A.** (2010) Nitrogen uptake, assimilation and remobilization in plants: challenges for sustainable and productive agriculture. *Annals of Botany*, **105**, 1141–1157.

McLoughlin, F., **Augustine, R.C.**, **Marshall, R.S.**, **Li, F.**, **Kirkpatrick, L.D.**, **Otegui, M.S.** ***et al.*** (2018) Maize multi-omics reveal roles for autophagic recycling in proteome remodelling and lipid turnover. *Nature Plants*, **4**, 1056–1070.

Nielsen, M.E., **Jurgens, G.** & **Thordal-Christensen, H.** (2017) VPS9a activates the Rab5 GTPase ARA7 to confer distinct pre- and Postinvasive plant innate immunity. *Plant Cell*, **29**, 1927–1937.

Nishimura, T. & **Tooze, S.A.** (2020) Emerging roles of ATG proteins and membrane lipids in autophagosome formation. *Cell Discovery*, **6**, 32.

Oliveira, I.C., **Brenner, E.**, **Chiu, J.**, **Hsieh, M.H.**, **Kouranov, A.**, **Lam, H.M.** ***et al.*** (2001) Metabolite and light regulation of metabolism in plants: lessons from the study of a single biochemical pathway. *Brazilian Journal of Medical and Biological Research*, **34**, 567–575.

Otasek, D., **Morris, J.H.**, **Boucas, J.**, **Pico, A.R.** & **Demchak, B.** (2019) Cytoscape automation: empowering workflow-based network analysis. *Genome Biology*, **20**, 185.

Paez Valencia, J., **Goodman, K.** & **Otegui, M.S.** (2016) Endocytosis and endosomal trafficking in plants. *Annual Review of Plant Biology*, **67**, 309–335.

Qi, H., **Li, J.**, **Xia, F.N.**, **Chen, J.Y.**, **Lei, X.**, **Han, M.Q.** ***et al.*** (2020) Arabidopsis SINAT proteins control autophagy by mediating ubiquitylation and degradation of ATG13. *Plant Cell*, **32**, 263–284.

Rajagopal, D. & **Mathew, M.K.** (2020) Role of Arabidopsis RAB5 GEF vps9a in maintaining potassium levels under sodium chloride stress. *Plant Direct*, **4**, e00273.

Reyes, F.C., **Buono, R.** & **Otegui, M.S.** (2011) Plant endosomal trafficking pathways. *Current Opinion in Plant Biology*, **14**, 666–673.

Reyes, F.C., **Buono, R.A.**, **Roschzttardtz, H.**, **Di Rubbo, S.**, **Yeun, L.H.**, **Russinova, E.** ***et al.*** (2014) A novel endosomal sorting complex required for transport (ESCRT) component in Arabidopsis thaliana controls cell expansion and development. *The Journal of Biological Chemistry*, **289**, 4980–4988.

Schneider, C.A., **Rasband, W.S.** & **Eliceiri, K.W.** (2012) NIH image to ImageJ: 25 years of image analysis. *Nature Methods*, **9**, 671–675.

Siodmak, A., **Shahul Hameed, U.F.**, **Rayapuram, N.**, **Volz, R.**, **Boudsocq, M.**, **Alharbi, S.** ***et al.*** (2023) Essential role of the CD docking motif of MPK4 in plant immunity, growth, and development. *The New Phytologist*, **239**, 1112–1126.

Spallek, T., **Beck, M.**, **Ben Khaled, S.**, **Salomon, S.**, **Bourdais, G.**, **Schellmann, S.** ***et al.*** (2013) ESCRT-I mediates FLS2 endosomal sorting and plant immunity. *PLoS Genetics*, **9**, e1004035.

Spitzer, C., **Li, F.**, **Buono, R.**, **Roschzttardtz, H.**, **Chung, T.**, **Zhang, M.** ***et al.*** (2015) The endosomal protein CHARGED MULTIVESICULAR BODY PROTEIN1 regulates the autophagic turnover of plastids in Arabidopsis. *Plant Cell*, **27**, 391–402.

Sun, X., **Jia, X.**, **Huo, L.**, **Che, R.**, **Gong, X.**, **Wang, P.** ***et al.*** (2018) MdATG18a overexpression improves tolerance to nitrogen deficiency and regulates anthocyanin accumulation through increased autophagy in transgenic apple. *Plant, Cell & Environment*, **41**, 469–480.

Sunada, M., **Goh, T.**, **Ueda, T.** & **Nakano, A.** (2016) Functional analyses of the plant-specific C-terminal region of VPS9a: the activating factor for RAB5 in Arabidopsis thaliana. *Journal of Plant Research*, **129**, 93–102.

Surpin, M., **Zheng, H.**, **Morita, M.T.**, **Saito, C.**, **Avila, E.**, **Blakeslee, J.J.** ***et al.*** (2003) The VTI family of SNARE proteins is necessary for plant viability and mediates different protein transport pathways. *Plant Cell*, **15**, 2885–2899.

Sutipatanasomboon, A., **Herberth, S.**, **Alwood, E.G.**, **Haweker, H.**, **Muller, B.**, **Shahriari, M.** ***et al.*** (2017) Disruption of the plant-specific CFS1 gene impairs autophagosome turnover and triggers EDS1-dependent cell death. *Scientific Reports*, **7**, 8677.

Suttangkakul, A., **Li, F.**, **Chung, T.** & **Vierstra, R.D.** (2011) The ATG1/ATG13 protein kinase complex is both a regulator and a target of autophagic recycling in Arabidopsis. *Plant Cell*, **23**, 3761–3779.

Takagi, M., **Hamano, K.**, **Takagi, H.**, **Morimoto, T.**, **Akimitsu, K.**, **Terauchi, R.** ***et al.*** (2019) Disruption of the MAMP-induced MEKK1-MKK1/MKK2-MPK4 pathway activates the TNL immune receptor SMN1/RPS6. *Plant & Cell Physiology*, **60**, 778–787.

Tang, J. & **Bassham, D.C.** (2022) Autophagy during drought: function, regulation, and potential application. *The Plant Journal*, **109**, 390–401.

The, S.V., **Snyder, R.** & **Tegeder, M.** (2020) Targeting nitrogen metabolism and transport processes to improve plant nitrogen use efficiency. *Frontiers in Plant Science*, **11**, 628366.

Thompson, A.R., **Doelling, J.H.**, **Suttangkakul, A.** & **Vierstra, R.D.** (2005) Autophagic nutrient recycling in Arabidopsis directed by the ATG8 and ATG12 conjugation pathways. *Plant Physiology*, **138**, 2097–2110.

Wada, S., **Hayashida, Y.**, **Izumi, M.**, **Kurusu, T.**, **Hanamata, S.**, **Kanno, K.** ***et al.*** (2015) Autophagy supports biomass production and nitrogen use efficiency at the vegetative stage in rice. *Plant Physiology*, **168**, 60–73.

Wang, H.J., **Hsu, Y.W.**, **Guo, C.L.**, **Jane, W.N.**, **Wang, H.**, **Jiang, L.** ***et al.*** (2017) VPS36-dependent multivesicular bodies are critical for Plasma-membrane protein turnover and vacuolar biogenesis. *Plant Physiology*, **173**, 566–581.

Wang, Y., **Li, J.**, **Wang, J.**, **Han, P.**, **Miao, S.**, **Zheng, X.** ***et al.*** (2022) Plant UVRAG interacts with ATG14 to regulate autophagosome maturation and geminivirus infection. *The New Phytologist*, **236**, 1358–1374.

Wen, L., **Fukuda, M.**, **Sunada, M.**, **Ishino, S.**, **Ishino, Y.**, **Okita, T.W.** ***et al.*** (2015) Guanine nucleotide exchange factor 2 for Rab5 proteins coordinated with GLUP6/GEF regulates the intracellular transport of the proglutelin from the Golgi apparatus to the protein storage vacuole in rice endosperm. *Journal of Experimental Botany*, **66**, 6137–6147.

Winter, V. & **Hauser, M.T.** (2006) Exploring the ESCRTing machinery in eukaryotes. *Trends in Plant Science*, **11**, 115–123.

Xia, F.N., **Zeng, B.**, **Liu, H.S.**, **Qi, H.**, **Xie, L.J.**, **Yu, L.J.** ***et al.*** (2020) SINAT E3 ubiquitin ligases mediate FREE1 and VPS23A degradation to modulate abscisic acid signaling. *Plant Cell*, **32**, 3290–3310.

Xing, J., **Cao, X.**, **Zhang, M.**, **Wei, X.**, **Zhang, J.** & **Wan, X.** (2023) Plant nitrogen availability and crosstalk with phytohormones signallings and their biotechnology breeding application in crops. *Plant Biotechnology Journal*, **21**, 1320–1342.

Xu, N., **Gao, X.Q.**, **Zhao, X.Y.**, **Zhu, D.Z.**, **Zhou, L.Z.** & **Zhang, X.S.** (2011) Arabidopsis AtVPS15 is essential for pollen development and germination through modulating phosphatidylinositol 3-phosphate formation. *Plant Molecular Biology*, **77**, 251–260.

Xue, H., **Zhou, W.**, **Yang, L.**, **Li, S.**, **Lei, P.**, **An, X.** ***et al.*** (2024) Endoplasmic reticulum protein ALTERED MERISTEM PROGRAM 1 negatively regulates senescence in Arabidopsis. *Plant Physiology*, **196**, 273–290.

Zeng, Y., **Li, B.**, **Huang, S.**, **Li, H.**, **Cao, W.**, **Chen, Y.** ***et al.*** (2023) The plant unique ESCRT component FREE1 regulates autophagosome closure. *Nature Communications*, **14**, 1768.

Zhang, J., **Buegger, F.**, **Albert, A.**, **Ghirardo, A.**, **Winkler, B.**, **Schnitzler, J.P.** ***et al.*** (2019) Phytoglobin overexpression promotes barley growth in the presence of enhanced level of atmospheric nitric oxide. *Journal of Experimental Botany*, **70**, 4521–4537.

Zhang, X., **Bai, S.**, **Min, H.**, **Cui, Y.**, **Sun, Y.** & **Feng, Y.** (2025) Evolutionary dynamics of nitrate uptake, assimilation, and signalling in plants: adapting to a changing environment. *Physiologia Plantarum*, **177**, e70069.

Zhao, J., **Bui, M.T.**, **Ma, J.**, **Kunzl, F.**, **Picchianti, L.**, **De La Concepcion, J.C.** ***et al.*** (2022) Plant autophagosomes mature into amphisomes prior to their delivery to the central vacuole. *The Journal of Cell Biology*, **221**, e202203139.

Zhou, F., **Zou, S.**, **Chen, Y.**, **Lipatova, Z.**, **Sun, D.**, **Zhu, X.** ***et al.*** (2017) A Rab5 GTPase module is important for autophagosome closure. *PLoS Genetics*, **13**, e1007020.

Zhou, Y., **Manghwar, H.**, **Hu, W.** & **Liu, F.** (2022) Degradation mechanism of autophagy-related proteins and research Progress. *International Journal of Molecular Sciences*, **23**, 7301.

Zhu, X.M., **Liang, S.**, **Shi, H.B.**, **Lu, J.P.**, **Dong, B.**, **Liao, Q.S.** ***et al.*** (2018) VPS9 domain-containing proteins are essential for autophagy and endocytosis in *Pyricularia oryzae*. *Environmental Microbiology*, **20**, 1516–1530.

Zhu, Y., **Zeng, Y.** & **Jiang, L.** (2024) FREE1 regulates phagophore closure in plants. *Autophagy*, **20**, 1452–1454.

Zhuang, X., **Wang, H.**, **Lam, S.K.**, **Gao, C.**, **Wang, X.**, **Cai, Y.** ***et al.*** (2013) A BAR-domain protein SH3P2, which binds to phosphatidylinositol 3-phosphate and ATG8, regulates autophagosome formation in Arabidopsis. *Plant Cell*, **25**, 4596–4615.